Planetary and Space Science 90 (2014) 37–59

Contents lists available at ScienceDirect

Planetary and Space Science

journal homepage: www.elsevier.com/locate/pss

Analysis of Rosetta/VIRTIS spectra of earth using observations from ENVISAT/AATSR, TERRA/MODIS and ENVISAT/SCIAMACHY, and radiative-transfer simulations

J. Hurley [a,*], P.G.J. Irwin [a], A. Adriani [b], M. Moriconi [c], F. Oliva [b], F. Capaccioni [b], A. Smith [a], G. Filacchione [b], F. Tosi [b], G. Thomas [a]

[a] Atmospheric, Oceanic and Planetary Physics, Clarendon Laboratory, Department of Physics, University of Oxford, Parks Road, Oxford OX1 3PU, UK
[b] Istituto di Astrofisica e Planetologia Spaziali, I-00133 Rome, Italy
[c] Istituto di Scienze dell'Atmosfera e del Clima, I-00133 Rome, Italy

ARTICLE INFO

Article history:
Received 8 February 2013
Received in revised form
13 June 2013
Accepted 13 June 2013
Available online 24 June 2013

Keywords:
Rosetta/VIRTIS
Atmospheres
Radiative transfer
Earth observation
Infrared
Comet

ABSTRACT

Rosetta, the Solar System cornerstone mission of ESA's Horizon 2000 programme, consists of an orbiter and a lander, and is due to arrive at the comet 67P/Churyumov–Gerasimenko in May 2014. Following its 2004 launch, Rosetta carried out a series of planetary fly-bys and gravitational assists. On these close fly-bys of the Earth, measurements were taken by the Visible Infrared Thermal Imaging Spectrometer (VIRTIS). Analysis of these spectra and comparison with spectra acquired by Earth-observing satellites can support the verification of the inflight calibration of Rosetta/VIRTIS.

In this paper, measurements taken by VIRTIS in November 2009 are compared with suitable coincident data from Earth-observing instruments (ESA-ENVISAT/AATSR and SCIAMACHY, and EOS-TERRA/MODIS). Radiative transfer simulations using NEMESIS (Irwin et al., 2008) are fit to the fly-by data taken by VIRTIS, using representative atmospheric and surface parameters. VIRTIS measurements correlate 90% with AATSR's, 85–94% with MODIS, and 82–88% with SCIAMACHYs.

The VIRTIS spectra are reproducible in the 1–5 μm region, except in the 1.4 μm deep water vapour spectral absorption band in the near-infrared in cases in which the radiance is very low (cloud-free topographies), where VIRTIS consistently registers more radiance than do MODIS and SCIAMACHY. Over these cloud-free regions, VIRTIS registers radiances a factor of 3–10 larger than SCIAMACHY and of 3–8 greater than MODIS. It is speculated that this discrepancy could be due to a spectral light leak originating from reflections from the order-sorting filters above the detector around 1.4 μm.

1. Introduction

Rosetta, as part of ESA's Horizon 2000 programme, consists of an orbiter and a lander and is due to arrive at the comet 67P/Churyumov–Gerasimenko in May 2014. Launched in March 2004, its trajectory has thus far mostly consisted of a series of planetary fly-bys and gravitational assists using Mars (2007) and Earth (2005, 2007 and 2009), and of fly-bys of two asteroids (2867 Steins and 21 Lutetia). During these close fly-bys Rosetta captured measurements of these asteroids and planets (Coradini et al., 2010, 2011; Tosi et al., 2010, 2012). In this study, the observations registered by the Visible Infrared Thermal Imaging Spectrometer (VIRTIS) of Earth, taken to verify and update the VIRTIS calibration, are discussed.

This work compares VIRTIS measurements from the third Earth fly-by with near-coincident radiometric data from operational Earth-observing instruments ENVISAT/AATSR, ENVISAT/SCIAMACHY and TERRA/MODIS (details thereof in Section 5). This set of VIRTIS measurements has been chosen because it is representative of the Earth fly-by dataset taken by VIRTIS, with integration times sufficient to resolve the well-known and well-characterised Earth spectrum over a range of surfaces and atmospheric properties. Additionally, the radiative transfer software NEMESIS (Section 4, Irwin et al., 2008) is employed to provide simulations to compare with the VIRTIS measurements (Section 6).

2. Rosetta/VIRTIS data: spectral region, geometry and noise

VIRTIS measures at high (although varying) spectral resolution from 0.25 to 5.0 μm, a spectral range which has been well studied

* Corresponding author. Current address: STFC Rutherford Appleton Laboratory, Harwell Science and Innovation Campus, Didcot OX11 0QX, UK.
Tel.: +44 1865 272895; fax: +44 1865 272923.
E-mail address: hurley@atm.ox.ac.uk (J. Hurley).

0032-0633/$ - see front matter © 2013 Elsevier Ltd. All rights reserved.
http://dx.doi.org/10.1016/j.pss.2013.06.012

by Earth observing instruments and thus is a good candidate for intercomparison studies (see Section 3).

VIRTIS covers three spectral regions with three independent detectors (Ammannito et al., 2006; Coradini et al., 2007):

1. *Mapper optical subsystem visible channel (M-VIS)*, 0.25–1 μm: A spectral mapper which images between 0.25 and 1 μm at a spectral sampling of 1.89 nm and a mean full-width-half-maximum (FWHM) of 2.11 nm, using a silicon charge coupled device (CCD);
2. *Mapper optical subsystem infrared channel (M-IR)*, 0.95–5 μm: A spectral mapper, imaging between 0.95 and 5 μm at a maximum spectral sampling of 9.45 nm and a mean FWHM of 12.6 nm, using a mercury cadmium telluride (HgCdTe) infrared focal plane array (IRFPA);
3. *High resolution optical subsystem (-H)*, 2–5 μm: A spectrometer, using an identical HgCdTe IRFPA, registering spectra between 2 and 5 μm at a resolution of 0.6 nm.

The two Mapper detectors share the same optical system which couples a Shafer telescope to an Offner spectrometer through a slit. The instantaneous field-of-view (FOV) of a single pixel is 250 μrad × 250 μrad, while the long rectangular slit covers an angular FOV of 250 μrad × 64 mrad. The instantaneous acquisition is a single frame which couples the spatial and spectral information, while the image itself is built in time, either in pushbroom mode or using an internal scan mechanism (Coradini et al., 2007). Thus, the standard product of the instrument is an 'image cube': a tridimensional matrix combining the spatial and spectral information. The spatial resolution is selected by either acquiring all the pixels or by averaging over a fixed number of 4 pixels, thus degrading the resolution to 1 mrad × 1 mrad. Moreover, the spectral data can be provided in two modes:

- 'High spectral resolution' mode: in which the initial spectral resolution of 9.45 nm is maintained;
- 'Nominal' mode: in which the 'high spectral resolution' mode measurements are averaged across three measurement bins to produce official VIRTIS-M spectra with spectral sampling of 28.35 nm.

Usage of the 'Nominal' versus 'High spectral resolution' modes shall be driven both by scientific needs and by the availability of resources of the spacecraft (data volume) — however during the main mission to the comet 67P, operations shall be carried out in 'high spectral resolution' mode in order to resolve narrow spectral features and to guarantee the maximum spatial resolution, using the onboard wavelet compression algorithms to reduce data volume (Langevin and Forni, 2000; Giuppi et al., 2011). Fig. 1 shows the FWHM of VIRTIS spectra above 1 μm, along with the actual instrument line shapes (ILS) at each of the central channel points for the 'high spectral' mode case. For the remainder of this work data obtained from the VIRTIS mapper infrared channel shall be exclusively used in both high and nominal spatial and spectral resolution modes.

There are known calibration issues below 1 μm (a systematic error which results in an increase in the perceived signal due to light from the higher negative orders of diffraction of the IR

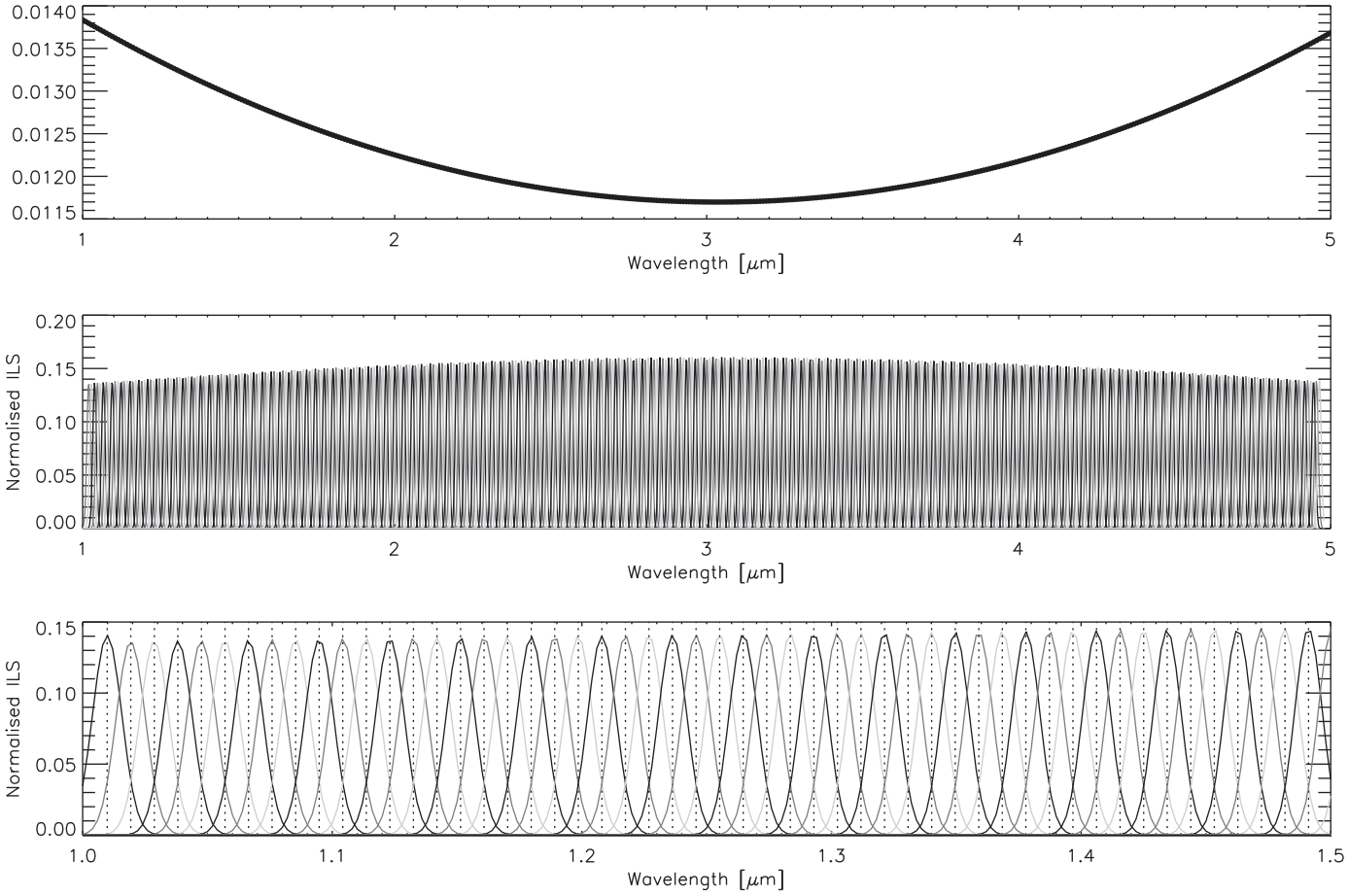

Fig. 1. Top panel shows FWHM at each spectral channel measured by VIRTIS' mapping optical system (M-IR), whilst bottom two plots show corresponding normalised Gaussian ILSs for each channel. Colours are used for visibility only, and the bottom plot is a zoom of the 1–1.5 μm region of the middle plot. Vertical dotted lines show central channel wavelengths.

grating being directed towards the visible detector). This contamination has an average level of 8% in the range 350–1000 nm (Filacchione et al., 2006). There are known calibration issues with the instrument, which could affect the retrieved radiances in parts of the overall IR spectral range. These are mainly caused by the presence of order sorting filters used to remove unwanted diffracted light from the grating of the instrument. For instance, thermal stresses within the Focal Plane Assembly after launch have caused a partial fissure at the junction between two of the order sorting filters mounted on the closure window of the detector, which results in reduced signal-to-noise (S/N) due to signal contamination by spurious reflections between 2.7 and 3.1 μm. This contamination affects the spatial information across about one-third of the 64 mrad-long slit in the spatial direction. In addition, there are documented excesses of signal between 1.415–1.594 μm and 2.5–2.7 μm, due to light scattered between adjacent order sorting filters. Finally, during this Earth fly-by the signal saturates at wavelengths in excess of 4.6 μm, for surface temperatures greater than about 290 K. The saturation is the result of a higher than nominal internal spectrometer temperature, due to the presence of the earth in the FOV of the panel radiator used to cool the spectrometer, and to the relatively long integration time used to maximise the signal in the 2.5–4 μm region.

Given these known issues, in this work the spectral range 1–5 μm will be considered, ignoring the 2.5–3.1 μm and 4.6–5.0 μm regions. This represents a wide spectral range in which VIRTIS is confirmed to provide accurate high resolution measurements, from which atmospheric and surface parameters can be expected to be precisely derived.

VIRTIS observations of Earth, during the third fly-by performed by Rosetta, are composed of a set of image cubes acquired at different spatial and spectral resolutions, and covering a range of different viewing and solar geometries. In the present analysis, two image cubes — one at the maximum spectral and spatial resolution, and the other at the reduced nominal resolution — are used, the details thereof which are given in Table 1. The observation in nominal mode is shown, as highlighted in Fig. 2 where the solar zenith, azimuth and emission angles for the selected observation of the third Earth fly-by (00216726958, over North Africa and the Atlantic) are shown. Such a large range of viewing geometries provides an interesting scope from a calibration perspective, providing a wide range over which to test the behaviour of the instrument.

The noise equivalent spectral radiance (NESR) has been calculated for a typical ocean pixel in the studied observation, using Earth-specific parameters. From this pixel, the NESR is generally 0.1% the measured signal registered by VIRTIS, giving a signal-to-noise (S/N) ratio of 1000 at each spectral point.

3. Identification of measured topography

A set of masks have been developed to distinguish between different topographies captured by the VIRTIS measurements of Earth — namely ocean, desert, vegetation, and clouds — using strong and consistent reflectance spectral features specific to the individual topographies. Fig. 3 shows, for observation 00216726958, the average measured ocean, desert, vegetation, and cloud spectra,

Table 1
Observation details of Rosetta/VIRTIS data used in this study, all taken on 13 November 2009.

Observation	Operative mode	Start time	Stop time	Mean distance to ground (km)	Ground resolution (km)	Spectral resolution (nm)
00216726248	High resolution	09:44:48	09:55:41	84 525	21	9.45
00216726958	Nominal, 4 × 3 bins	09:56:38	10:07:31	91 265	91	28.35

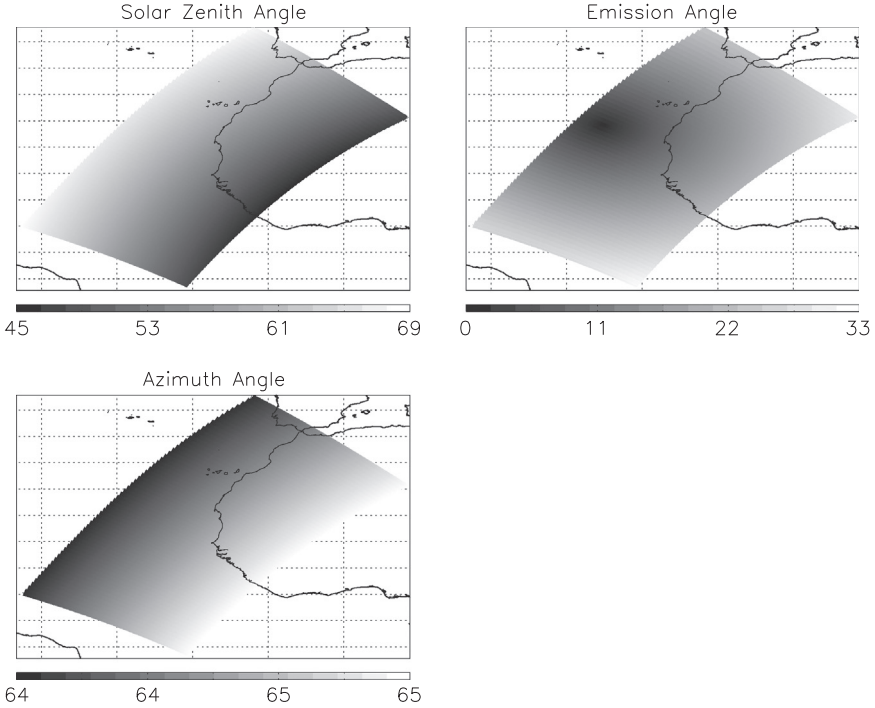

Fig. 2. Solar zenith angle (top left), emission angle (top right) and azimuth angle (bottom left) for measurements taken by VIRTIS observation 00216726958.

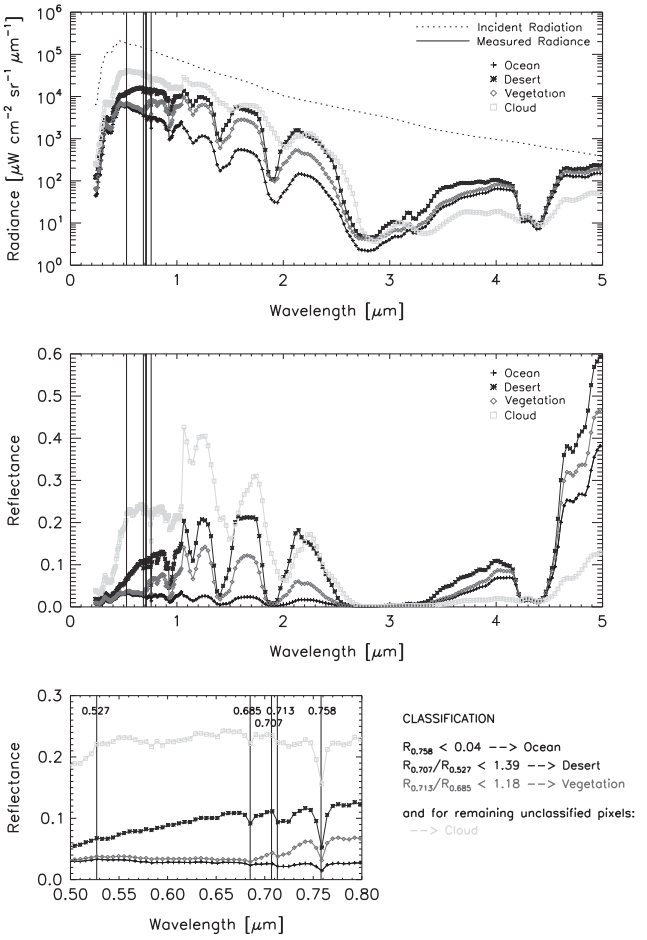

Fig. 3. Average radiance measurements (top) for each topography given in colour, and corresponding reflectance spectra (middle), with mask spectral-locations given by dark vertical lines. Zoom of spectral region in which masks are defined (bottom left). Specifics of spectral masks detailed in bottom right panel.

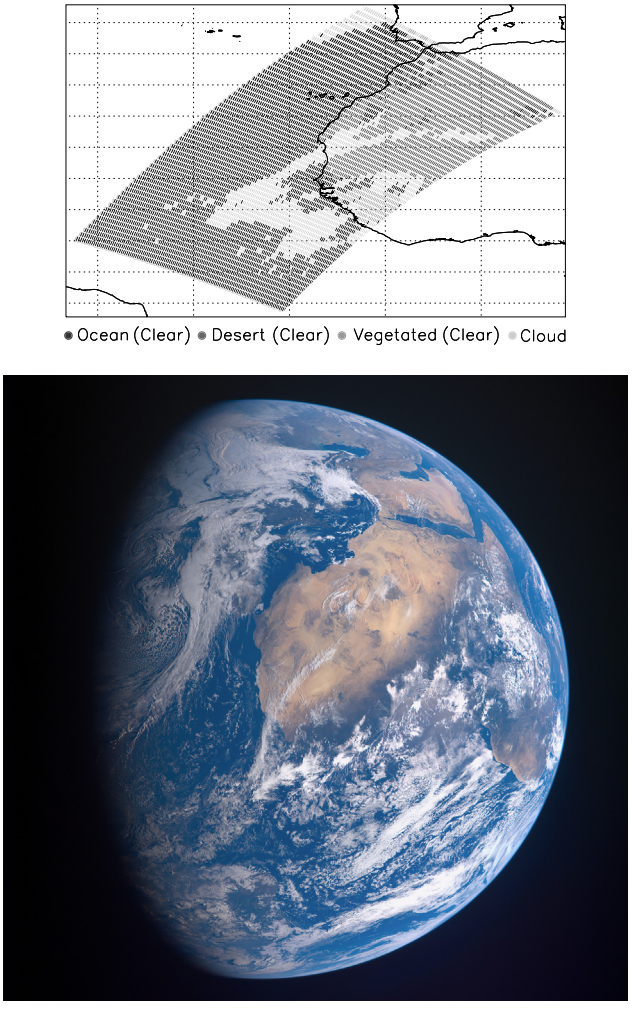

Fig. 4. Top panel: Application of topographical mask to VIRTIS observation 00216726958. Bottom panel: Rosetta/OSIRIS coincident Wide Angle Camera colour-image (acknowledgement: H. Sierks of MPS, Katlenburg-Lindau, Germany, and the European Space Agency).

as well as the calculated incident radiation. It shows the average reflectance spectra thus calculated, and highlights the spectral features used in the topographical spectral masks, along with the details of the reflectance criteria for these masks. Fig. 4 shows the resulting topographical mask for the observation, along with a coincident Rosetta/OSIRIS Wide Angle Camera near true-colour image. The VIRTIS topography mask agrees well with the topographical features visible in the matching OSIRIS image, with the VIRTIS mask missing small-scale scattered clouds over ocean.

4. Radiative transfer tool and input parameters

NEMESIS (the Non-linear Optimal Estimator for Multivariate Spectral Analysis) is used as the radiative transfer code, as well as the tool used to invert spectral measurements using a correlated-*k* optimal-estimation retrieval algorithm (Irwin et al., 2008). Correlated-*k* is employed because calculating atmospheric spectra using individual line strengths and widths is computationally expensive, and it is often sufficiently accurate to reformulate the absorption coefficients (k) within a particular spectral range into *k*-distributions (Lacis and Oinas, 1991; Goody et al., 1989). These inverse cumulative frequency distributions of the absorption coefficients are pre-calculated on a temperature/pressure grid appropriate for Earth's atmosphere — and are known as *k*-tables — which allow for quick computation times since these *k*-tables are tabulated with fewer points than that of the spectral resolution. NEMESIS was originally developed to interpret observations of Saturn and Titan from Cassini/CIRS, but has been generalised to apply to any planetary atmosphere, and has been applied to many planetary missions and observations. In this application, line-data (from which *k*-tables are calculated) is taken from HITRAN-2004 (Rothman et al., 2005) and atmospheric data is provided by ENVISAT/MIPAS reference atmospheres (Remedios, 2001).

Furthermore, as the measurement viewing geometries are not limb, there will be significant emission from the surface captured by the measurements, and hence it is important to well-characterise the surface albedo. A priori surface albedo spectra are taken from the ASTER spectral library (Baldridge et al., in press), for each topography. The desert surface albedo is an average of all sampled sand types assessed, whilst the vegetation surface albedo is representative of a deciduous forest. The ocean albedo is a salt-water reflectance, which is available only above 2 μm — and so is extended below 2 μm using fresh-water reflectances, as outside regions of sun-glint (specular reflection) the ocean is expected to be quite black. It should be noted that, whilst it is expected that the ocean albedo will be fairly black, there will be varying contributions from sun-glint, wind-ruffled water, and chlorophyll concentrations which can be modelled (Sayer et al., 2010) — however for the purposes of this work, the

surface reflectance is taken from ASTER, and not modified to represent the specific conditions. It must be recalled, however, that the albedo value given in the ASTER database represents a directional hemispherical reflectance, whilst a bidirectional reflectance is required, rather, in this work, leading to potential differences of more than a factor of two (Hapke, 1984). Fig. 5 shows the surface reflectances taken as a priori for each of the surface topographies.

5. Comparison with ENVISAT/AATSR, TERRA/MODIS and ENVISAT/SCIAMACHY

The Advanced Along-Track Scanning Radiometer (AATSR, Llewellyn-Jones et al., 2001) and the Scanning Imaging Absorption Spectrometer for Atmospheric Cartography (SCIAMACHY, Burrows et al., 1995), onboard ESA-ENVISAT, as well as the Moderate Resolution Imaging Spectroradiometer (MODIS), onboard EOS-TERRA (King et al., 1992) provide spectrally, geographically and temporally coincident data to that taken by VIRTIS, albeit at different spatial and spectral resolutions. These 'coincident' data have measurement time differences of up to 2 h — however, at the scale at which the comparison is carried out, and beyond shifting of localised cloud boundaries, are sufficiently close in time and space to be considered coincident. In all cases, the compared spectral data have been convolved with the same instrument line shape (whichever is wider in the comparison) in order to have the data on the same spectral grid, and all data has been averaged onto the same spatial latitude/longitude grid for spatial compatibility — with the caveat that the information content of remote sensing images is not independent of the native measurement scale determined by the spatial resolution of the sensor. These coincidences are limited to the surface footprints, and there is expected to be some variability in the exact location of tropospheric clouds whose sharp edges are likely to move in that timeframe. Comparison of AATSR, SCIAMACHY, and MODIS radiances with those measured by VIRTIS can give insight into the behaviour and quality of the VIRTIS measurements, assuming that the four instruments sample the same atmosphere.

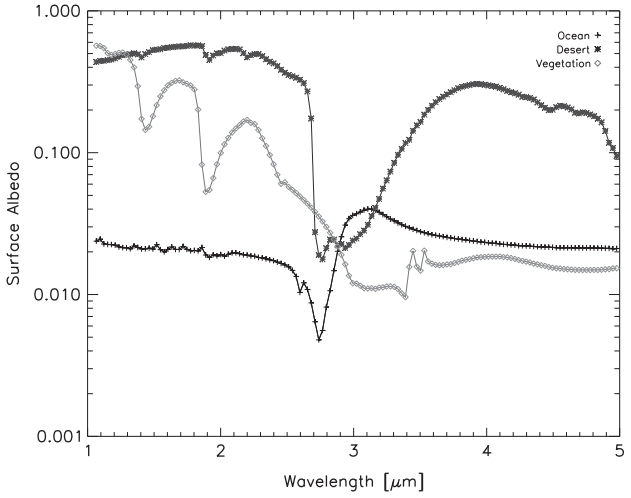

Fig. 5. Surface albedo for ocean, desert and vegetation.

Table 2
AATSR channels. Overlapping channels are given in italics.

Channel number	Wavelength (μm)	Measured quantity
1	0.55	Reflectance
2	0.66	Reflectance
3	0.87	Reflectance
4	*1.6*	*Reflectance*
5	*3.7*	*Brightness temperature*
6	11	Brightness temperature
7	12	Brightness temperature

5.1. ENVISAT/AATSR

ENVISAT/AATSR measures reflectance and brightness temperature (as appropriate) in seven channels distributed through the visible and infrared (Table 2), to within an accuracy of 0.5 K in the infrared over ocean, and to within about 3% in the visible (Llewellyn-Jones et al., 2001). AATSR measures at 10:00 am local solar time, and completes global coverage every 3 days, having a spatial resolution of 1 km at nadir in a swath 500 km wide. AATSR measurements taken on the same day as measured by VIRTIS are considered, with AATSR measuring at 11:45 TC in a spatially coincident swath in the VIRTIS region of interest. It is asserted that both instruments then should have sampled approximately the same atmosphere since VIRTIS measured the region between 9:56 am and 10:07 am UTC.

The AATSR channels at 1.6 μm and 3.7 μm overlap with the VIRTIS spectral range, having spectral responses as shown in Fig. 6. These filter responses are applied to VIRTIS data, and finally both datasets are averaged on the same latitude/longitude grid to account for different spatial and spectral resolutions. AATSR data have been converted into units of radiance (from reflectances (1.6 μm) and brightness temperatures (3.7 μm)) for comparison with VIRTIS measurements.

The viewing geometry of each individual pixel in the VIRTIS dataset is slightly different, and each pixel in each AATSR swath is measured at two different viewing geometries (nadir, and forward-viewing at 55°). NEMESIS has been used to simulate the radiance emitted at both 1.6 μm and 3.7 μm to investigate the effect of changing emission angle upon radiance measured by the instruments, for each of the topographies identified by VIRTIS (Fig. 7). This confirms that for all topographies other than cloud,

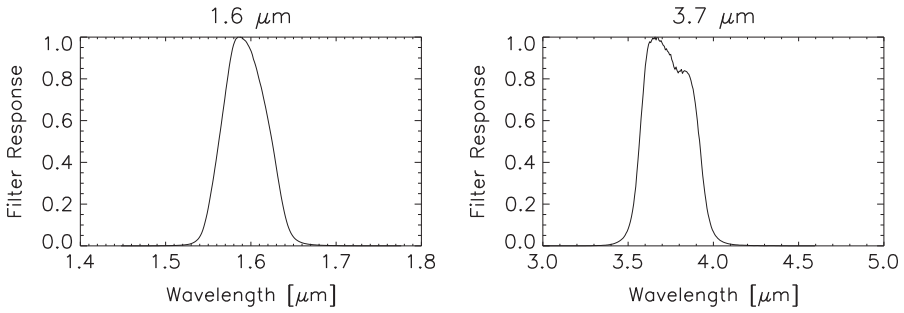

Fig. 6. Spectral response of AATSR filters, for channels at 1.6 μm and 3.7 μm.

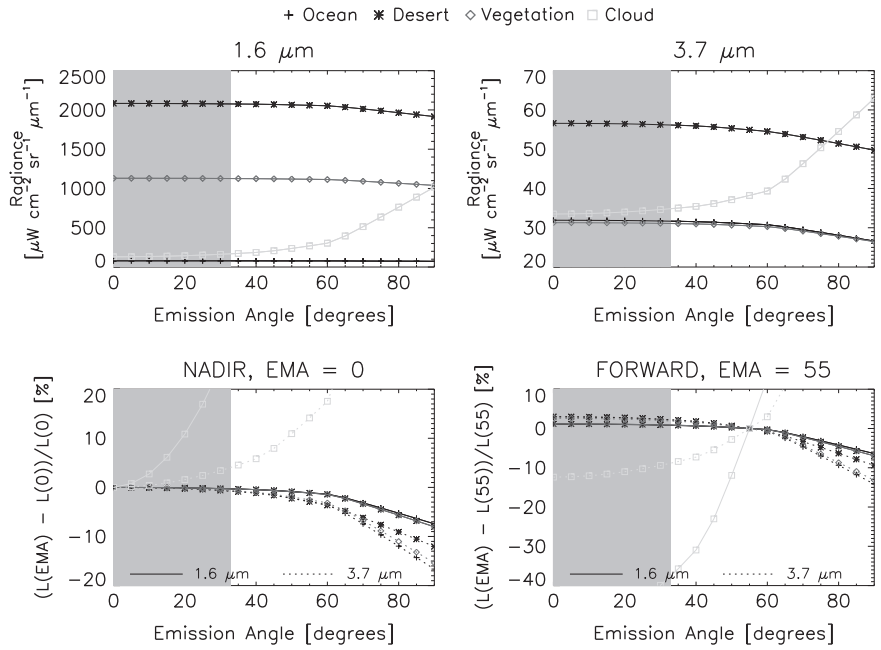

Fig. 7. Top panels: Pencil-beam radiances for emission angles between nadir and limb extremes of viewing geometry, at 1.6 μm (left) and 3.7 μm (right), for each of the identified VIRTIS topologies (colours). Bottom panels: The relative difference between a nadir (left panel) or 55° emission angle (right panel) measurement, and those taken at emission angles between nadir and limb, at 1.6 μm (solid lines) and 3.7 μm (dotted lines), for each topography (colours). Grey regions highlight those emission angles sampled by VIRTIS.

emission angle makes negligible difference below about 60°. Since the current studied VIRTIS image has emission angles between nadir and about 33°, the nadir AATSR measurements are used, and are expected to vary by less than approximately 1%.

Fig. 8 shows the results of this comparison. The two instruments certainly do appear to see the same atmosphere, as even synoptic conditions such as clouds are visible in similar geographical locations in the radiance fields. When the average radiance in each latitude/longitude grid-box is calculated, given the appropriate filter response functions, the overlapping measurements taken by both AATSR and VIRTIS agree with a correlation coefficient of 0.9 at 1.6 μm and 0.9 at 3.7 μm. This implies that VIRTIS measures reliably in window regions of the spectrum, both in the near and thermal infrared.

5.2. TERRA/MODIS

MODIS takes nadir measurements in 36 channels (nine of which overlap with the spectral range of VIRTIS, Table 3) in the visible and infrared, with a spatial resolution varying between 250 m and 1 km in a 2330 km-wide swath — however in this analysis, products aggregated at 1 km resolution are used. In the visible and near-infrared, MODIS measures reflected solar radiation (good to within 2%) which are calibrated to radiance measurements (good to within 5%) using an onboard solar diffuser (King et al., 1992). In the mid- through thermal infrared, MODIS measures thermal emission — which has a noise equivalent difference temperature error of about 0.25 K (King et al., 1992), but is known to suffer particularly from stripe noise (Rakwatin et al., 2007).

TERRA/MODIS measures at 10:30 am local solar time, moving from north-to-south whilst AQUA/MODIS measures at 1:30 pm local solar time, orbiting south-to-north. The combination of TERRA and AQUA MODIS measurements completes global coverage in less than 2 days. For the purposes of this comparison, only those measurements registered by TERRA/MODIS are considered using three consecutive orbits spanning 10:10 am–1:30 pm UTC (and thus, for the remainder of this work 'MODIS' refers to TERRA/MODIS), with most of the VIRTIS swath covered with a 1:45–2 h time difference. Given this time difference, to a reasonable extent, it can be assumed that both these instruments sample approximately the same atmosphere, with the exception of highly mobile tropospheric features such as cloud edges.

Considering Fig. 9, which shows the RGB composite of the region of interest, produced using a combination of appropriate MODIS visible channel measurements, it does appear that MODIS and VIRTIS do indeed see approximately the same atmosphere despite the discrepancy in measurement time, as even short-lived and mobile features such as clouds are in the same relative position in both images. Study of the image also suggests that the VIRTIS topographical mask misses many scattered small clouds over the ocean, as well as over vegetated regions, which is expected since the cloud mask was designed to isolate high ice clouds, as well as given the time discrepancy between the two observations. The differences can be accounted for if the large differences between the spatial resolutions of the selected images for MODIS (1×1 km) and VIRTIS (91×91 km) are considered, since the information content of remote sensing images is not independent of the native measurement scale determined by the spatial resolution of the sensor. Degradation of the spatial resolution scale reduces the contrast in features, thus causing an underestimation of small scale and fragmented features such as the small clouds in the present images (Nelson et al., 2009; Marceau et al., 1994).

Again, as MODIS measurements are taken at nadir geometry, there should be negligible differences due to viewing geometry except for cloudy pixels, as discussed in Fig. 7. VIRTIS spectra have been convolved across MODIS' spectral bandpass for each overlapping band (Fig. 10), and both datasets have been regridded onto a common latitude/longitude grid of spatial resolution similar to that of VIRTIS, as shown in Figs. 11 and 12.

MODIS radiances match VIRTIS and AATSR radiances in the window regions (1.23–1.25 μm, 1.628–1.652 μm, 2.105–2.155 μm, 3.66–3.84 μm) throughout the spectra (except for cloudy regions, in which measurement geometry becomes important), with MODIS and VIRTIS measurements correlating generally at about

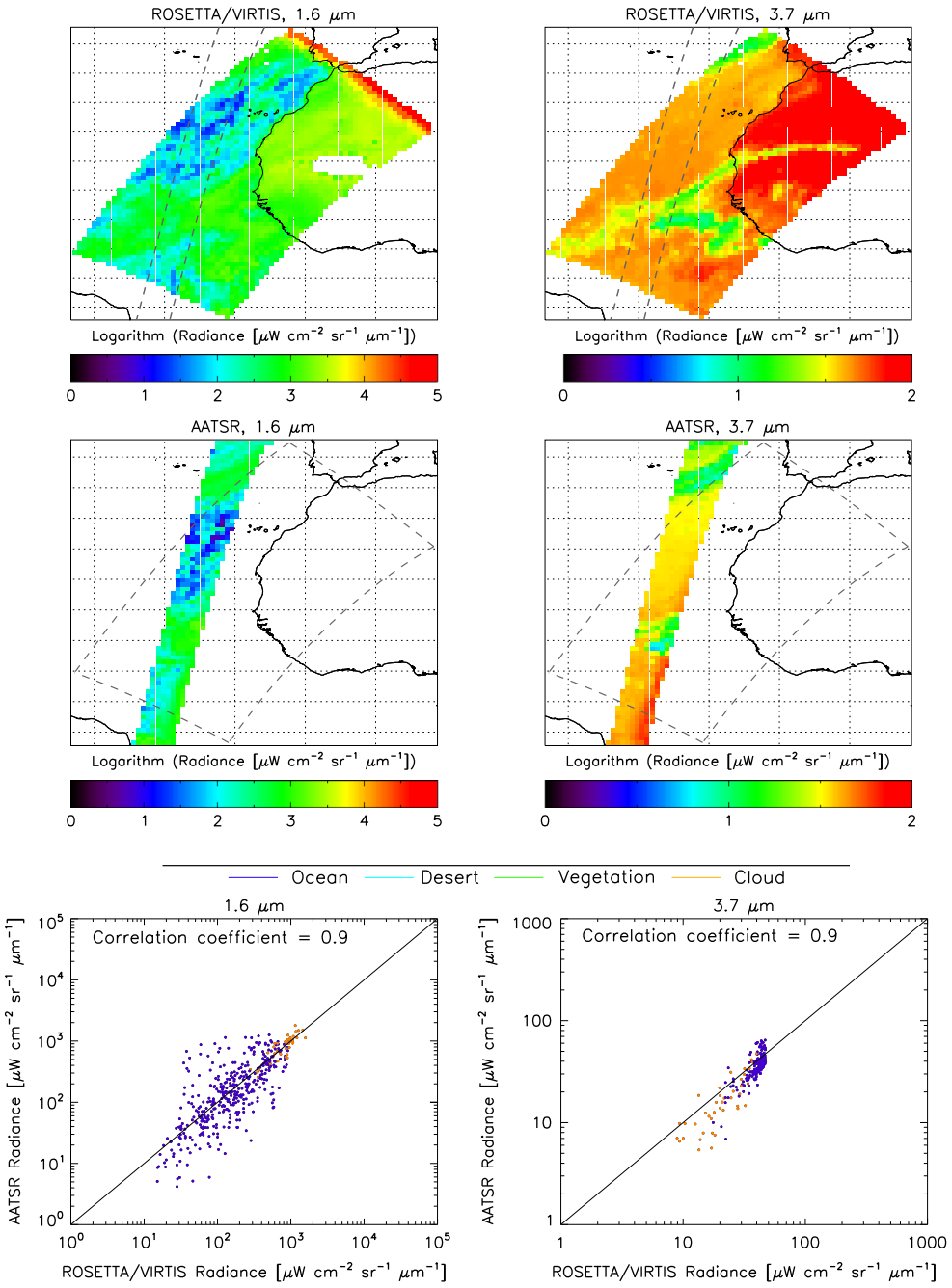

Fig. 8. Comparison of VIRTIS and AATSR radiances. Top panels: VIRTIS radiances, at 1.6 μm (left) and 3.7 μm (right), with the grey dashed rectangle showing the boundary of AATSR swath. Middle panels: AATSR radiances, at 1.6 μm (left) and 3.7 μm (right), with the grey dashed rectangle showing the boundary of VIRTIS swath. Bottom panels: Scatterplot of VIRTIS and AATSR radiances at each latitude/longitude grid-box, with each topography given in a different colour, at 1.6 μm (left) and 3.7 μm (right).

the 90% level. The correlation becomes slightly worse at thermal wavelengths, with correlation generally dropping to between 85% and 88%, and with MODIS channel 24 (4.433–4.498 μm) showing an apparent uncorrected flat-field effect (which appears as a decrease in detected radiances at the edges of its FOV). It is interesting to note, although expected, the inversion in the radiance level between ocean and desert pixels in contrast with that between high and low cloud pixels. In the solar reflection region, the clouds have generally larger radiances than the ocean/desert pixels, while the reverse is true starting from channel 20 (3.66–3.84 μm), marking the start of the thermal radiance spectral region. Additionally, from Fig. 12 it appears that the larger discrepancies between MODIS and VIRTIS radiances in the thermal emission windows can be directly correlated to the radiances measured in the clouds. This discrepancy is explained by the large variation in native spatial resolution of the MODIS and VIRTIS data; in fact, the sub-pixel distribution of thermal radiance sources strongly affects the overall pixel radiance. In this spectral range the average radiance calculated from MODIS cannot be simply weighted by the pixel area but also requires that the temperature of the single source regions (the temperature in the single MODIS pixels) be taken into account. This detailed evaluation goes beyond the scope of this paper and will not be discussed further.

However, in the water vapour absorption region measured in MODIS' channel 26 at 1.36–1.39 μm (Fig. 11 second panel from top), sandwiched between window regions at 1.24 μm and

Table 3
MODIS channels. Overlapping channels are given in italics.

Channel number	Wavelength (μm)	Type
1	0.620–0.670	Solar reflective
2	0.841–0.876	Solar reflective
3	0.459–0.479	Solar reflective
4	0.545–0.565	Solar reflective
5	*1.230–1.250*	*Solar reflective*
6	*1.628–1.652*	*Solar reflective*
7	*2.105–2.155*	*Solar reflective*
8	0.405–0.420	Solar reflective
9	0.438–0.448	Solar reflective
10	0.483–0.493	Solar reflective
11	0.526–0.536	Solar reflective
12	0.546–0.556	Solar reflective
13	0.662–0.672	Solar reflective
14	0.673–0.683	Solar reflective
15	0.743–0.753	Solar reflective
16	0.862–0.877	Solar reflective
17	0.890–0.920	Solar reflective
18	0.931–0.941	Solar reflective
19	0.915–0.965	Solar reflective
20	*3.660–3.840*	*Thermal emissive*
21	*3.929–3.989*	*Thermal emissive*
22	*3.929–3.989*	*Thermal emissive*
23	*4.020–4.080*	*Thermal emissive*
24	*4.433–4.498*	*Thermal emissive*
25	*4.482–4.549*	*Thermal emissive*
26	*1.360–1.390*	*Solar reflective*
27	6.535–6.895	Thermal emissive
28	7.175–7.475	Thermal emissive
29	8.400–8.700	Thermal emissive
30	9.580–9.880	Thermal emissive
31	10.780–11.280	Thermal emissive
32	11.770–12.270	Thermal emissive
33	13.185–13.485	Thermal emissive
34	13.485–13.785	Thermal emissive
35	13.785–14.085	Thermal emissive
36	14.085–14.385	Thermal emissive

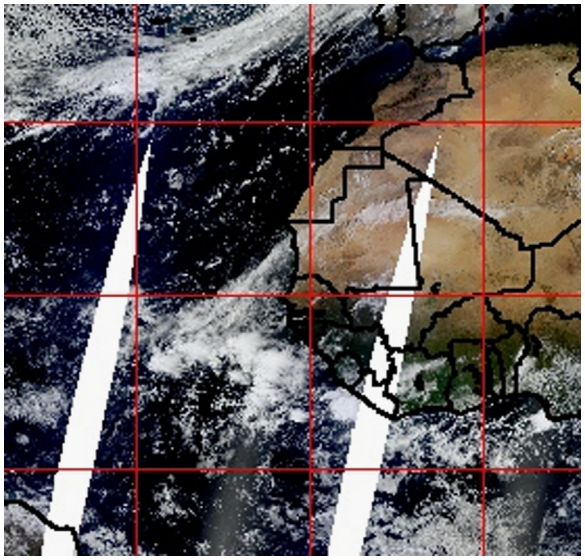

Fig. 9. Visible composite of the region of interest, provided from combination of visible spectral range of the coincident MODIS measurements (NASA, 2010).

1.64 μm, MODIS consistently measures the depth of the absorption feature 2–10 times deeper than does VIRTIS over desert, vegetation and cloud-free ocean pixels and over a wide interval of radiance levels.

The difference is clearly evident in the projected images where VIRTIS radiances delineate the coastline (in cloud-free regions) while MODIS shows no land/ocean boundary, continuing the low

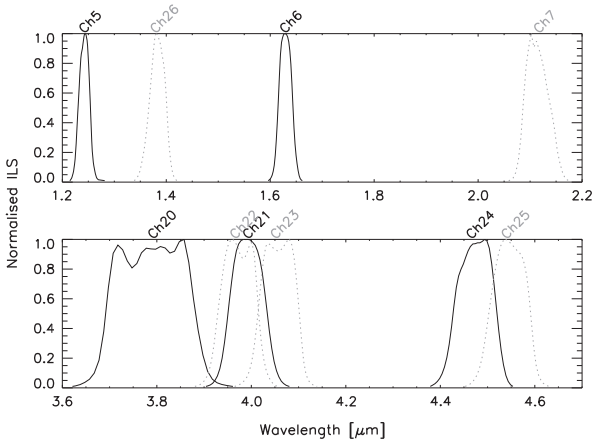

Fig. 10. MODIS normalised instrument line shapes (ILS) for each of the overlapping channels split into two wavelength ranges for visibility.

radiance levels over land, as expected as this water vapour channel should not be sensitive to the surface. The VIRTIS data, showing a clear tracing of the coastline, and distinct water abundances across the land/ocean boundary, are indicative of a light leak across the spectral domain of VIRTIS near the 1.4 μm water vapour absorption feature. As mentioned already in Section 2, this is the location of the boundary between two order sorting filters.

5.3. ENVISAT/SCIAMACHY

ENVISAT/SCIAMACHY is a grating spectrometer, measuring emitted radiance in eight bands (each consisting of 1024 channels, spaced at nearly 40 times the 'nominal mode' spectral resolution of VIRTIS) distributed through the visible and infrared range, and measures polarisation in seven channels spread over nearly the same spectral range (Table 4). SCIAMACHY scans in three modes: cross-track, limb and solar/lunar occultation — but for this comparison, only nadir measurements are used, having a spatial resolution of 16 km × 32 km in a swath of 1000 km. SCIAMACHY is on the same platform as AATSR, with a local solar time of 10:00 am corresponding to ≈11:45 am UTC within the VIRTIS swath region, so the temporal shift is similar to that of the AATSR comparisons.

SCIAMACHY has, for this comparison, the advantage of measuring continuously at a high spectral resolution in the shortwave and near-infrared regions of the spectrum. Thus, in conjunction with the relative depths of the water absorption features at 1.15 μm and 1.4 μm, the spectral shape over a range of near-infrared wavelengths can be assessed. However, there is a known light leak in the 1.940–2.040 μm band (which currently renders atmospheric retrievals from the band impossible) and suspected ice contamination of varying severity in the ranges of 1.000–1.750 μm (channel 6), 1.940–2.040 μm (channel 7) and 2.265–2.380 μm (channel 8) bands (ESA, 2008). For the purposes of comparison, only the spectral band spanning 1.000–1.750 μm is studied (keeping in mind the possible contamination) — and furthermore, the SCIAMACHY data has been smoothed to the same spectral resolution as VIRTIS using the VIRTIS ILSs shown in Fig. 1.

5.3.1. Comparison with 'nominal mode' VIRTIS measurements

Fig. 13 shows the coincident 'nominal mode' VIRTIS measurements with SCIAMACHY data, at each VIRTIS spectral point whilst Fig. 14 shows several sample ocean spectra — in both cases having degraded the SCIAMACHY spectra to VIRTIS (nominal) spectral resolution, and having regridded both onto the same spatial grid. Generally, the radiance in the window regions of the near-infrared

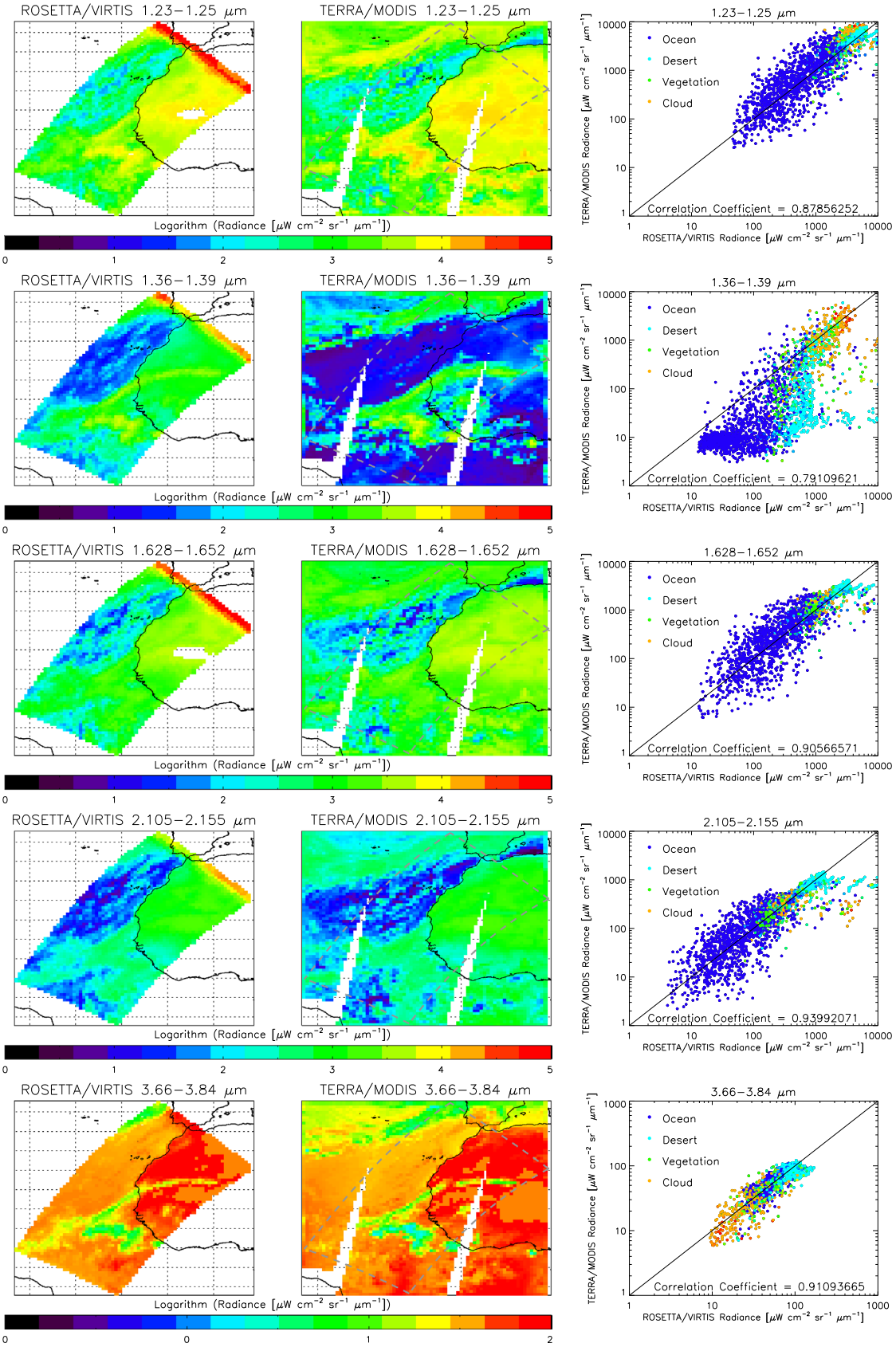

Fig. 11. Comparison of VIRTIS 'nominal mode' and MODIS radiances. VIRTIS (left column) and MODIS (midle column) radiances, at each of the appropriate overlapping MODIS channels (each channel is a row). Grey dashed rectangle in MODIS plots show boundary of VIRTIS swath. Right column shows scatterplot of average radiance in each latitude/longitude grid-box, colour-coded by topography. Note that not all colour scales are the same in this figure.

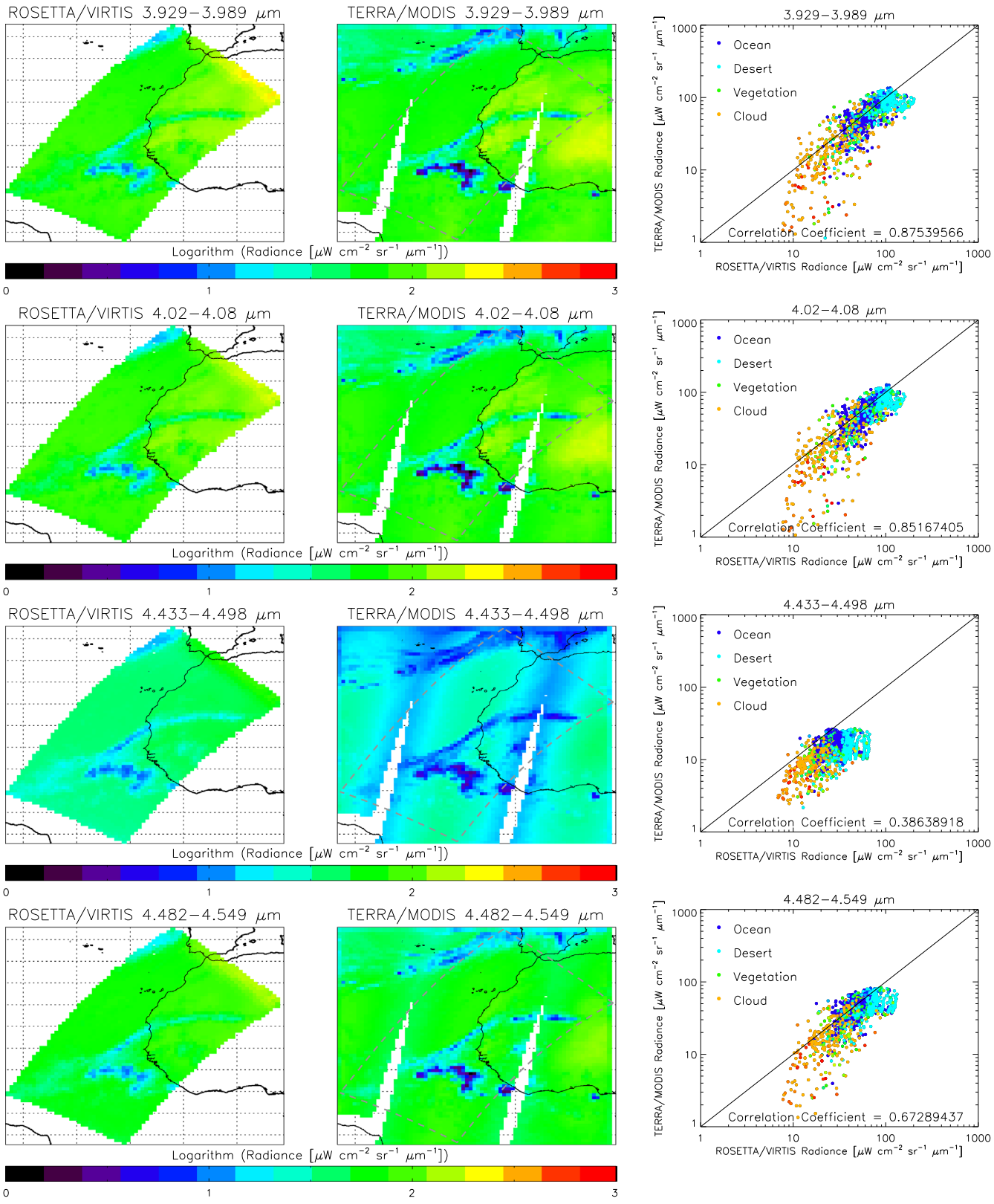

Fig. 12. As described in Fig. 11, for rest of MODIS channels.

is similar in magnitude for both instruments, with a correlation between the two sets of coincident measurements generally at about the 85% level — however, the absorption features measured by SCIAMACHY (at 1.15 μm and 1.4 μm) are noticeably far deeper in cloud-free regions than those measured by VIRTIS — up to 10–15 times, in fact. The MODIS comparison suggests this

Table 4
SCIAMACHY bands. Overlapping channels are given in italics.

Band wavelength (μm)	Number of channels	Spectral resolution (nm)	Measured quantity
0.240–0.314	1024	0.24	Radiance
0.309–0.405	1024	0.26	Radiance
0.394–0.620	1024	0.44	Radiance
0.604–0.805	1024	0.48	Radiance
0.785–1.050	1024	0.54	Radiance
1.000–1.750	*1024*	*1.48*	*Radiance*
1.940–2.040	*1024*	*0.22*	*Radiance*
2.265–2.380	*1024*	*0.26*	*Radiance*
0.310–2.380	7	67–137	Polarisation

underestimation of the absorption depth as well — although perhaps not quite as deeply as SCIAMACHY, which may have slight ice contamination.

In cloudy regions the two instruments measure nearly identical radiances, both in window and absorption spectral locations: this is because the continuum radiance emitted by clouds effectively fill-in any absorption features in spectra, and raise the radiance baseline, limiting to continua at the opaque limit (e.g. Hurley et al., 2011). Because of this, there is far more radiance measured in the water vapour absorption spectral regions than there would be in cloud-free conditions and hence any small deviations in signal are negligible in comparison with the cloudy signature whilst they appear to be the dominant radiance source in cloud-free cases.

5.3.2. *Comparison with 'high spectral resolution mode' VIRTIS scans*

As introduced previously, VIRTIS also measured higher spectral resolution spectra (at one-third the 'nominal' VIRTIS spectral resolution) at 9:44 am on the same day. On this particular observation, VIRTIS measurements were performed in 'high spatial and spectral resolution mode', resulting in similar spatial resolution for both VIRTIS (23×23 km) and SCIAMACHY (16×32 km). Comparison of these observations minimises the possibility of misinterpretations due to the different scales of the images, as is possible for the VIRTIS/MODIS comparison, as well as assessing if the differences between instruments could be an artifacts of spectral resolution or of the spectral-averaging method.

The 'high spectral resolution' VIRTIS data is compared with the nearest coincident SCIAMACHY observations (those introduced in Section 5.3). There is worse coincidence between these datasets due to the offset in measurement times than for the 'nominal' VIRTIS observation studied thus far, however the synoptic conditions such as cloud features seem not to have shifted significantly, although there are slight positional changes near sharp cloud edges. Fig. 15 shows the coincident 'high spectral resolution mode' VIRTIS and SCIAMACHY data, at each VIRTIS spectral point, and Fig. 16 shows several sample cloud-free spectra (all SCIAMACHY cases here are taken over the ocean) for this comparison using 'high spectral resolution mode' VIRTIS data. It is immediately observable from Fig. 15 that the excess signal at 1.4 μm previously discussed in the VIRTIS measurements is still evident in the 'high spectral resolution mode' measurements, but that the extra radiance in the 'nominal mode' measurements at 1.15 μm is not as evident in most of the spectra taken in the 'high spectral resolution' data.

Fig. 17 shows an overview of the VIRTIS spectra taken in the 'nominal' and 'high spectral resolution' modes, as well as the coincident SCIAMACHY spectra degraded to match the corresponding spectral resolutions. If there were no systematic components of noise or signal errors, it would be expected that roughly 50% of the SCIAMACHY measurements would be larger than the coincident VIRTIS measurement, and that about 50% would be smaller. For the continuum portions of the spectra, this proves to be largely the case — however, in the two water absorption features (1.15 μm and 1.4 μm), SCIAMACHY sees lower radiances in 75% and nearly 100% of cases for the 'nominal' spectral-resolution measurements, and in 60% and nearly 100% of cases for the 'high spectral resolution' measurements, for the same two absorption features. This behaviour is visible in the other sample spectra given in this figure. The 'high resolution spectra' seem better able to reproduce the SCIAMACHY radiance at 1.15 μm, suggesting that the averaging over spectral bins is the explanation for the signal excess at 1.15 μm. However, the signal excess at 1.4 μm is maintained in most of the 'high spectral resolution' VIRTIS spectra. This is particularly visible in Fig. 18, in which the radiance fields are plotted for the 'high spectral resolution' data, at two different wavelengths: 1.1 μm (window) and 1.37 μm (in 1.4 μm absorption feature). At 1.1 μm, the radiances from the two instruments are very similar, with a fairly random distribution of variances about the 1:1 line. At 1.37 μm, the larger values of radiance (attributed to the cloud features in the image) are again scattered randomly about the 1:1 line; however the smaller radiances corresponding to clear atmospheric measurements over ocean are considerably offset from the 1:1 line,with nearly 99% of all measurements having VIRTIS's radiance larger than that measured by SCIAMACHY. The dataset has been organised in Fig. 18 to show the scatter and distribution (1) when all coincident points are used, (2) when only the VIRTIS topographical masked 'ocean' pixels are used, and (3) when a subset of these ocean points are selected by eye from the image as not having any obvious cloud contamination. It appears that VIRTIS does not measure radiances less than approximately 10 $\mu W\,cm^{-2}\,sr^{-1}\,\mu m^{-1}$ in a spectral bin near 1.4 μm, whereas SCIAMACHY measures radiances of 2 $\mu W\,cm^{-2}\,sr^{-1}\,\mu m^{-1}$ (and MODIS 4 $\mu W\,cm^{-2}\,sr^{-1}\,\mu m^{-1}$).

Finally, it warrants to compare both the (high resolution) VIRTIS and SCIAMACHY together in the MODIS channels, as shown in Fig. 19, keeping in mind the time differences among the three sets of measurements and that there are only spatially coincident measurements between all three instruments over the ocean. Fig. 19 shows that overall SCIAMACHY and MODIS agree in that the radiances measured by VIRTIS in the 1.4 μm absorption band are too great, although the MODIS depths are not always quite as large as those measured by SCIAMACHY, manifesting in discrepancies between the lowest radiance levels measured by SCIAMACHY and those measured by MODIS, which could be a result of potential small water residues on SCIAMACHY's optics. If this is the case, the discrepancy between SCIAMACHY and VIRTIS radiances would be overestimated. Furthermore, the high-resolution VIRTIS data is able to somewhat reduce the discrepancy between it and MODIS/SCIAMACHY datasets from the nominal mode data shown in Fig 11, although there is still a notable discrepancy. VIRTIS never measures radiances lower than 10 $\mu W\,cm^{-2}\,sr^{-1}\,\mu m^{-1}$, overestimating the radiance of SCIAMACHY by a factor of 3–10, and that of MODIS by a factor of about 3–8.

5.4. *Intercomparison of coincident earth-observation data*

For completeness, it warrants to compare the coincident AATSR, MODIS and SCIAMACHY data themselves, to check whether they measure the same radiance. It is not possible to intercompare AATSR and MODIS since their discrete channels are non-overlapping. However, both AATSR and MODIS can be compared with SCIAMACHY by convolving the SCIAMACHY spectra with the appropriate instrument-specific channel functions, and regridding onto the same spatial grid, as shown in Fig. 20, for the near-infrared channels of AATSR and MODIS.

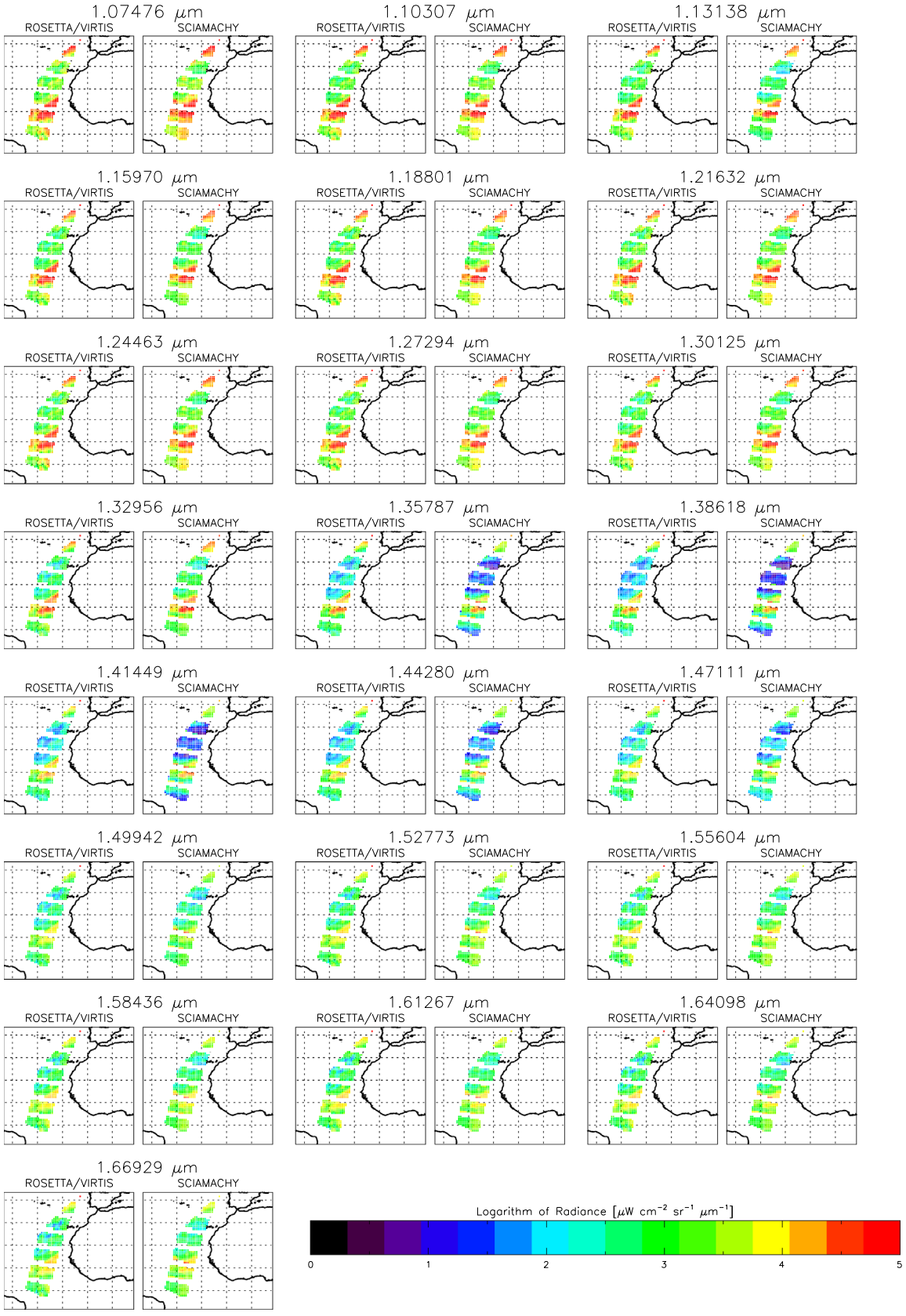

Fig. 13. Radiances measured in coincident 'nominal mode' VIRTIS (left) and SCIAMACHY (right) data. Each pair of plots is for particular wavelength.

Generally, MODIS and SCIAMACHY measurements are well correlated, although there are scattering of points near cloudy regions in which SCIAMACHY measures higher radiance, and there are discrepancies at the lowest range of registered SCIAMACHY radiances, which possibly can be attributed to small water residues on SCIAMACHY's optics. SCIAMACHY and AATSR are quite well

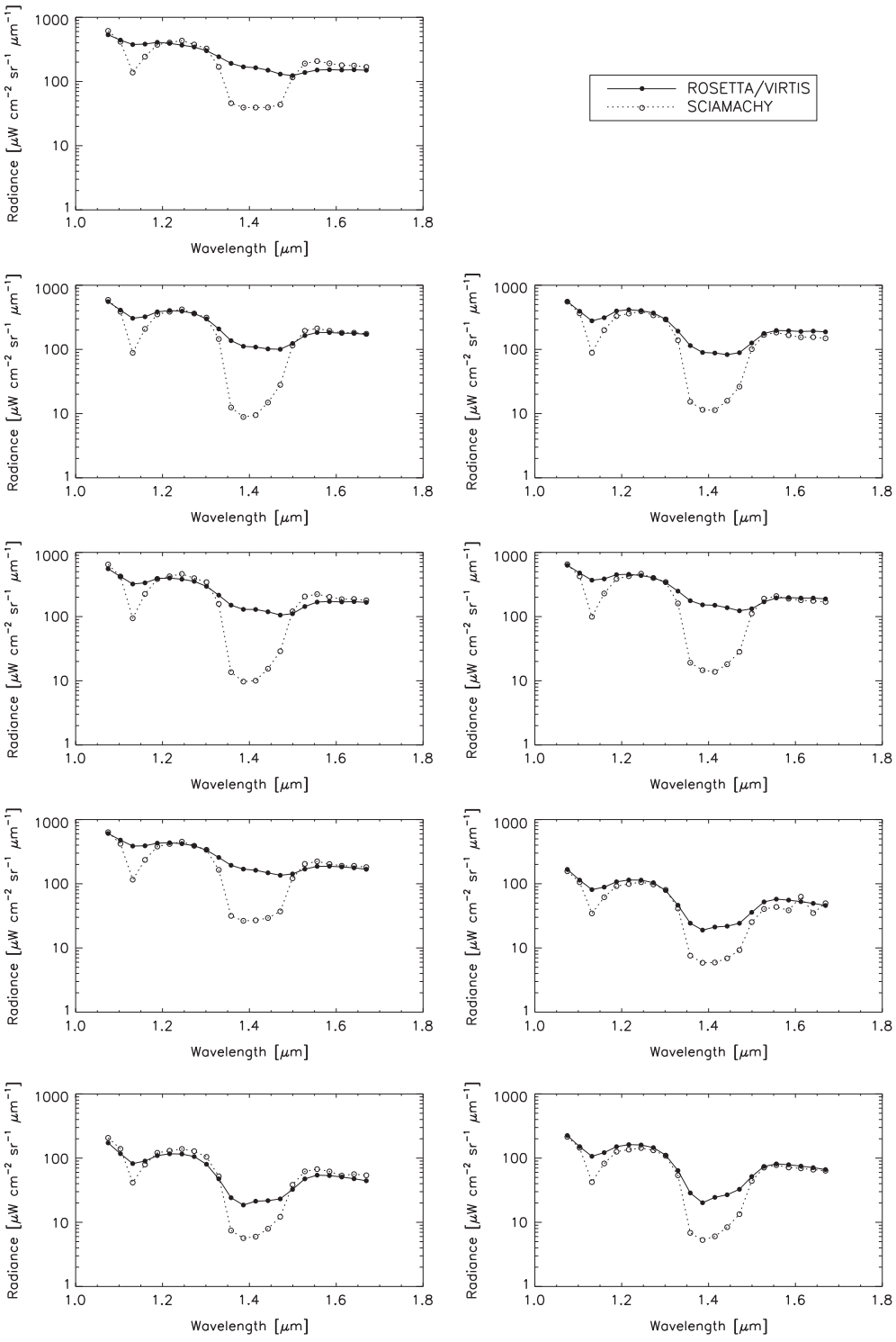

Fig. 14. A selection of ten sample spatially coincident ocean spectra, taken by VIRTIS in 'nominal mode' (solid line) and SCIAMACHY (dotted line).

correlated, although with a correlation coefficient of 0.76 which is lower than 90% correlation between VIRTIS and AATSR, with a smaller relative scatter. Furthermore, the SCIAMACHY and AATSR measurements are almost uniformly offset by a factor of about 3 to each other.

6. Cloud-free pixels: simulations

In this section, a typical cloud-free ocean grid-box (from Section 5.3) is studied — although it should be noted that such tropical regions are likely to have high/thin hazes or low/thin maritime aerosols present — and in this particular case, as discussed in Section 7, there was indeed stratospheric volcanic aerosol present at the mid-north-latitudes, due to the Sarychev eruption a few months before June 2009. However, comparison with limb-viewing ENVISAT/MIPAS and Odin/OSIRIS level 2 volcanic aerosol products indicates that on 13 November 2009 the volcanic aerosol was not present in the cloud-free ocean region of the VIRTIS observation, being further north (eg. Bourassa et al., 2012). Infrared limb-viewers are extremely sensitive to aerosol — even high, thin aerosols — due to their long pathlengths, and

Fig. 15. Radiances measured in coincident 'high spectral resolution' mode VIRTIS (left) and SCIAMACHY (right) data. Each pair of plots is for particular wavelength.

identify the highest layer of opacity, as shown in Fig. 21 for ENVISAT/MIPAS. In Fig. 21, the volcanic aerosol opacity is clearly visible in the northern mid-latitudes, skimming the top of the tropopause (being flagged as thin 12–15 km clouds, green/yellow open squares in online version), with a similar cloud field to those observed in the VIRTIS/MODIS/SCIAMACHY observations clearly

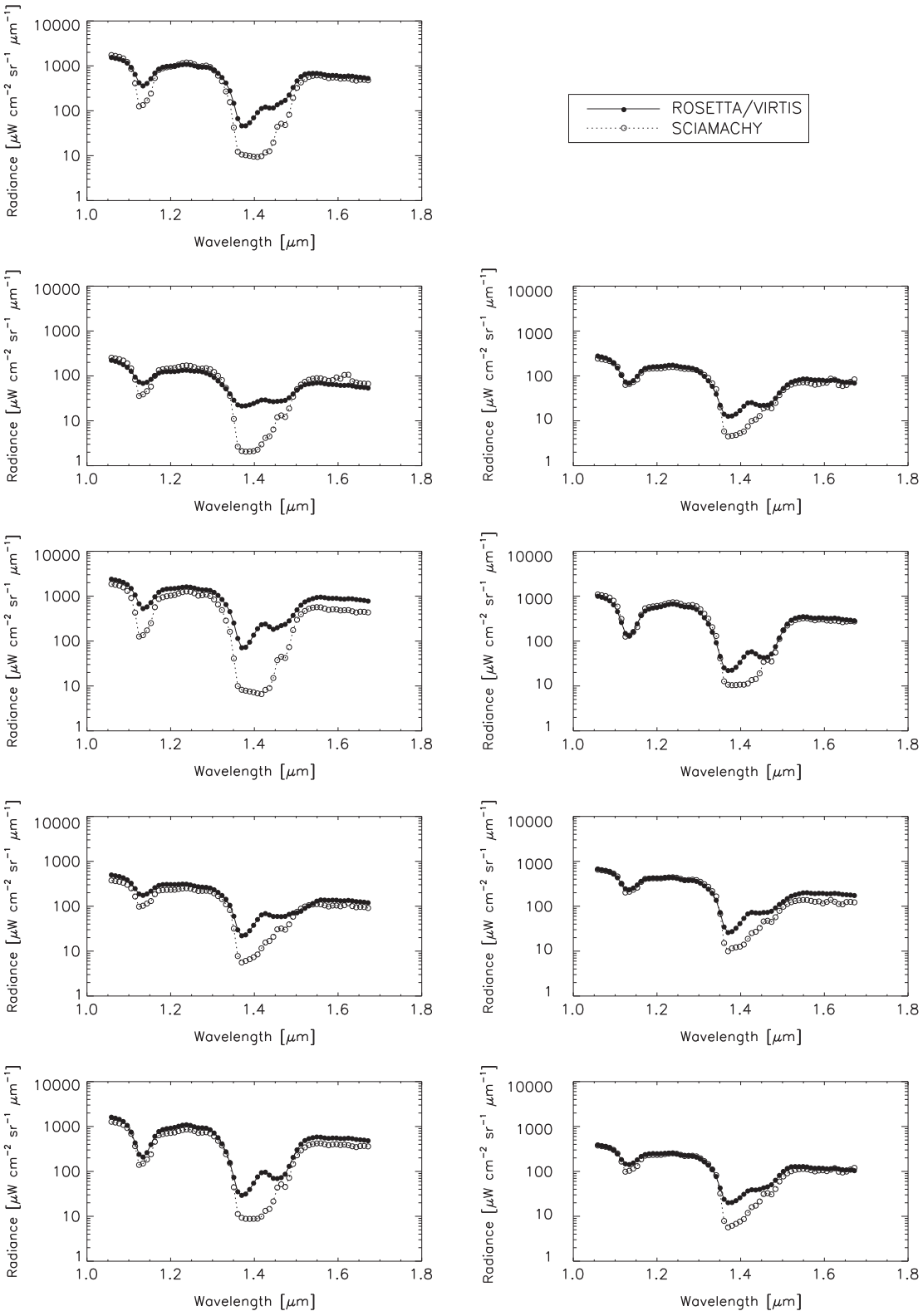

Fig. 16. A selection of ten sample spatially coincident ocean spectra, taken by VIRTIS in 'high spectral resolution mode' (solid line) and SCIAMACHY (dotted line) convolved to the VIRTIS 'high spectral resolution mode' ILS.

visible (yellow points in online version correspond to the clouds visible in the VIRTIS measurements), and red crosses indicating opacity-free measurement to 6 km (the lowest tangent height operationally registered by MIPAS) in the VIRTIS cloud-free ocean region of interest. Since MIPAS would pick up any higher aerosol, and since the opacity retrieval finds no aerosol above 6 km, it is extremely unlikely that there exists stratospheric volcanic aerosol (or any aerosol, for that matter) above this region. These results

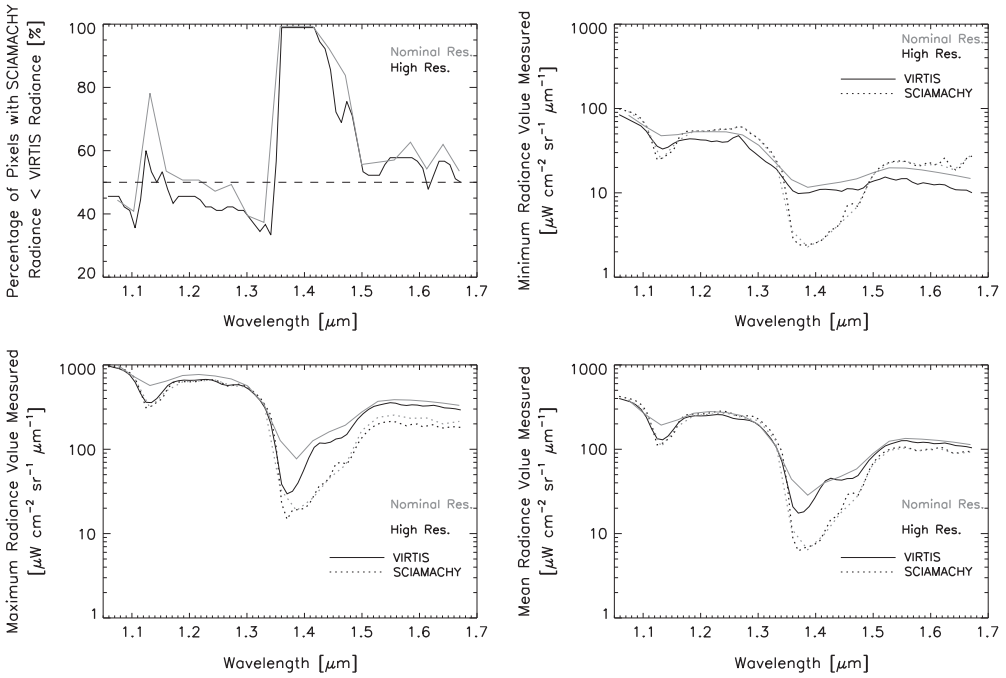

Fig. 17. Left top panel: Percent of measurement pixels for which the SCIAMACHY radiance is less than the corresponding VIRTIS radiance, as a function of wavelength, with 'nominal' spectral resolution in grey and 'high spectral resolution' in black. The dashed line shows the 50% level. Next three panels show comparison of SCIAMACHY (dotted) and VIRTIS (solid) measurements in 'nominal' (grey) and 'high spectral resolution' (black) observation modes: Minimum (top right), maximum (bottom left) and average (bottom right) radiance spectra in coincident SCIAMACHY and VIRTIS datasets.

are corroborated by Bourassa et al. (2012) using OSIRIS — Fig. 22 shows the OSIRIS aerosol extinction profiles at 750 nm in the region, showing opacities at background magnitudes.

Both VIRTIS and SCIAMACHY spectra from this grid-box are considered, at the nominal spectral-resolution of VIRTIS. MODIS level 2 products (temperature, water vapour concentration, and a low maritime haze of optical depth of approximately 0.1 at 550 nm) for the same grid-boxes are then input into the fully scattering NEMESIS model, along with climatological CO_2 from Remedios (2001) and suitable spectrally varying surface albedo (Baldridge et al., in press), and the simulated spectra calculated, whilst allowing the water vapour profile to be retrieved (Fig. 23). In these simulations, the OSIRIS aerosol extinction profile is used, with aerosol scattering properties corresponding to H_2SO_4 (the stratospheric aerosol present in very low background concentrations).

The radiative transfer simulations do a fairly good job of reproducing the average radiance measured by SCIAMACHY in the grid-box between 1.06 and 1.66 μm, retrieving the water from the SCIAMACHY measurements. However, starting with the VIRTIS 'nominal mode' measurements, and the same OSIRIS aerosol distribution, it is necessary to significantly decrease the concentration of tropospheric water vapour in order to approach the initial measurements — and in fact, in order to get a good fit, the optical depth of the aerosol must be increased tenfold as well (not shown).

Whilst MODIS and SCIAMACHY can be used more reliably to retrieve water vapour, this exercise highlights the difficulty of estimating water vapour from VIRTIS nominal mode data from this flyby (although not used in this example calculation, the high-resolution data suffer the same problem), since the retrieved VIRTIS water vapour concentration is very different from that calculated from either MODIS or SCIAMACHY. It should again be noted that it is likely that SCIAMACHY suffers slight water contamination, as its measured absorptions in the water bands are sometimes stronger than MODIS — the calculation below (in Fig. 24) is given as an example of the impact on retrieved water vapour that could result from light leaks near the 1.4 μm feature, combined with the nominal spectral resolution mode, which proves inappropriate for retrieving trace species concentrations.

Taking the retrieved water vapour profile derived from SCIAMACHY, and assuming the OSIRIS aerosol distribution, temperature and CO_2 profiles as applied previously, it is interesting to perturb the concentration of the tropospheric water vapour from this retrieved profile to study the effect on the depth of the 1.4 μm absorption radiance. The retrieved profile has a water vapour VMR of 0.0014 at 500 mbar. The measured SCIAMACHY radiance at 1.4 μm should — and does — match the radiance simulated at 1.4 μm using this retrieved water vapour profile. By matching the radiance measured by the typical VIRTIS observation to the simulated spectra representing different tropospheric VMR perturbations, what VMR the retrieval would choose for the particular radiance at 1.4 μm can be estimated. For instance, for the particular case studied, nominal mode VIRTIS observations would result in retrieving only 5% the tropospheric water vapour concentration as would the SCIAMACHY radiances — or, if SCIAMACHY's radiances are believed, only 5% the tropospheric water vapour concentration that VIRTIS should retrieve if there were not some instrument error (this is for proof of method only — it is not asserted here that SCIAMACHY radiances are the ground truth). If this is indeed the case, there will be an impact upon the water vapour content retrieved from the 1.4 μm water vapour absorption feature measured by VIRTIS, at least for extremely low radiance levels — and this could be a difficult issue to rectify. Generally as the apparent light leaks become larger (and hence more problematic, for instance over the land pixels where the shoulder continuum levels are large), the errors in retrieved water vapour concentrations will reflect these discrepancies correspondingly. It may well be, however, that an adjustment of some sort could be introduced as a 'correction' to such regions, which could enable water vapour retrievals. Such analysis is, however, beyond the scope of the current work. These results, however, warrant further investigation, as water (vapour and ice) is the dominant volatile in comets, which will be quantified by Rosetta/VIRTIS.

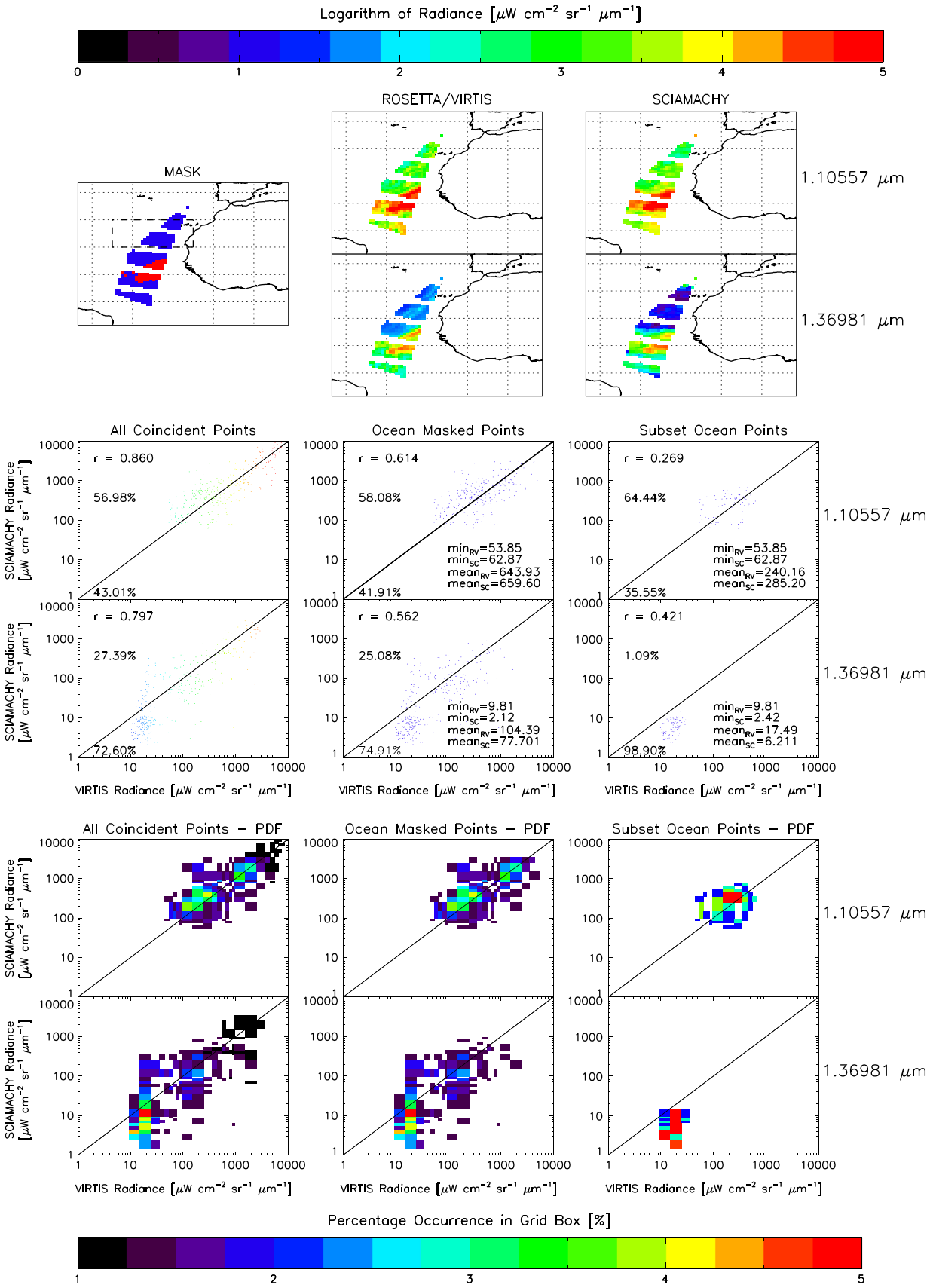

Fig. 18. Top row of panels: Radiances measured by 'high spectral resolution mode' VIRTIS (middle) and SCIAMACHY (right) at 1.1 μm (top) and 1.37 μm (bottom). Left plot shows VIRTIS' topographical mask, with clear ocean in blue, and cloud in red, and the subset of ocean points chosen by eye to not contain cloud given in a dashed box. Middle row of panels: Scatterplots of VIRTIS and SCIAMACHY radiances at 1.1 μm (top) and 1.37 μm (bottom). 'r' gives the correlation coefficient of the data, and the percentages above and below the 1:1 (black) line gives the percentage of data above and below the line. This is done for all coincident points (left), only ocean-masked points (middle) and for the chosen subset of visibly cloud-free ocean points (right). Bottom row of panels: as for middle set of panels, but giving the probability distribution functions (PDFs) showing the density of points in the scatterplots above.

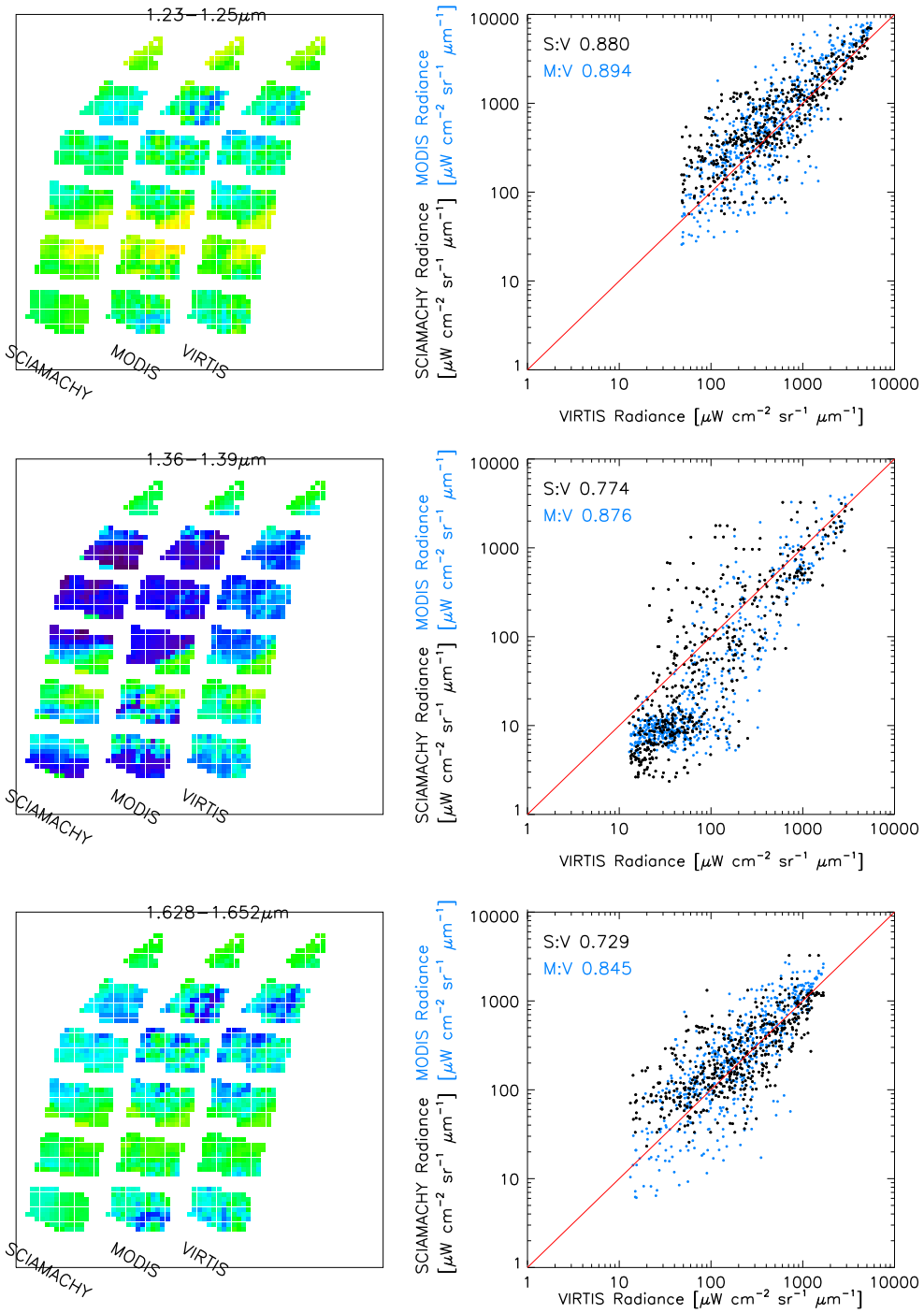

Fig. 19. Left panels give SCIAMACHY (left), MODIS (middle) and VIRTIS (right) radiances in the MODIS channel, with each row for a different channel. Right panels give pixel-by-pixel scatterplots of these channel radiances, with SCIAMACHY:VIRTIS in black and MODIS:VIRTIS in blue, with respective correlation coefficient noted.

7. Hypothesis upon apparent excess signal visible in low radiance measurements

There appears to be a fairly consistent overestimation of radiance measured by VIRTIS in the 1.4 μm water absorption band (as well as in the 1.15 μm band if the nominal spectral mode is used) when the observation is low radiance (i.e. cloud-free measurements). However, given the estimated S/N ratios — in excess of 1000 (Section 2) — if the relative depths of the water vapour absorption features at 1.15 μm by SCIAMACHY are believed, it would be expected that the feature at 1.15 μm would be 3–4 times deeper/smaller, and that at 1.4 μm it would be about 3–15 times smaller than what VIRTIS measures in its 'nominal mode' from SCIAMACHY and MODIS — in which case, the NESR values are not big enough to account for this effect. Furthermore, if random noise were the culprit for the decreased depth of these absorption features, the depths of the absorption features would vary from spectrum to spectrum — which they do not, over the subset of affected pixels. Finally, whilst the temporal shift of 1:30–2 h between VIRTIS and the Earth-observation instruments affects the observed radiances of the scene, the statistically consistent deviation at 1.4 μm but good correlation at other wavelengths

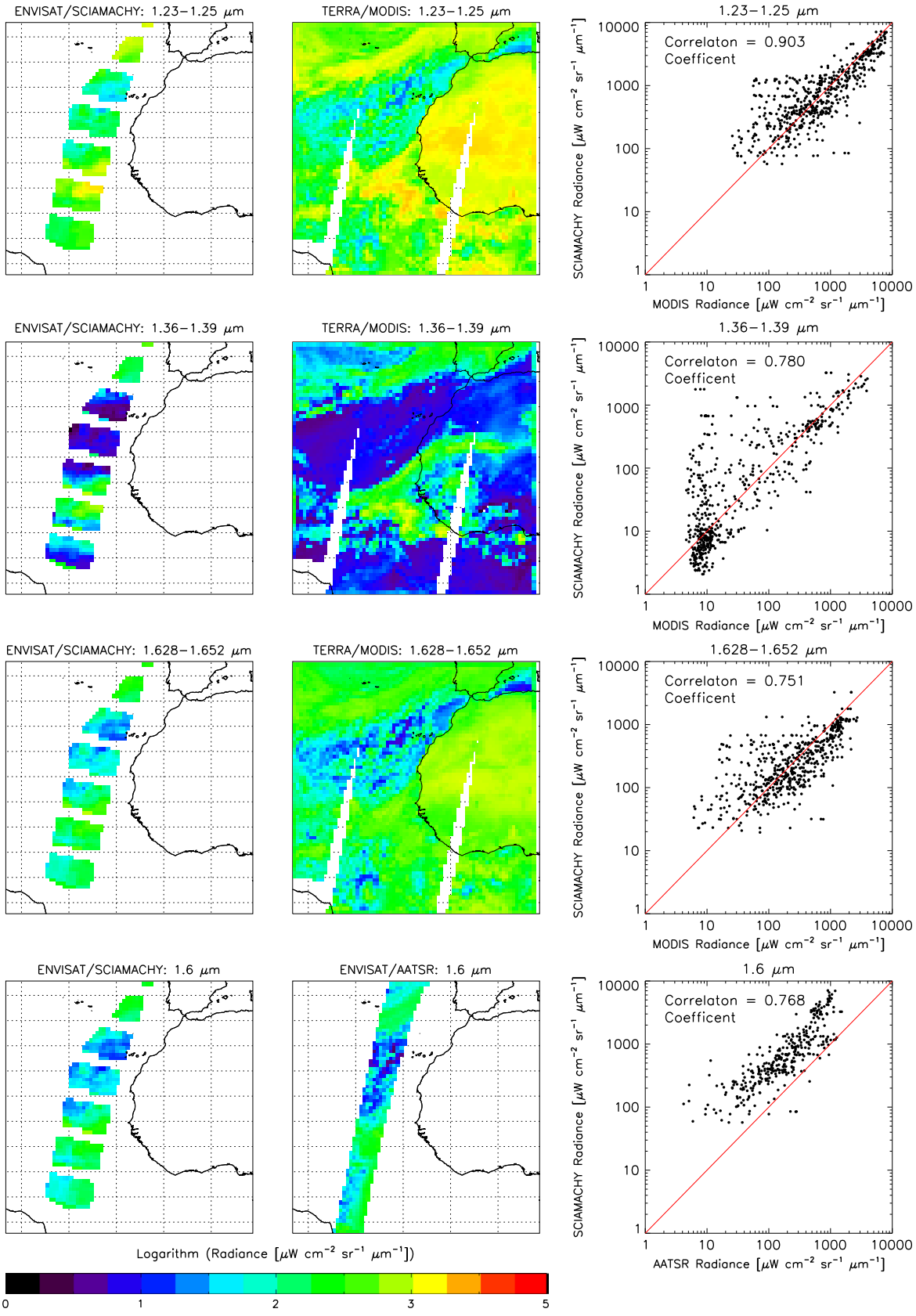

Fig. 20. Comparison of SCIAMACHY (left panels) and MODIS (middle) in MODIS' near-infrared channels (top 3 rows, channel noted in title), and SCIAMACHY (left) and AATSR (middle) in AATSR's near-infrared channel (bottom row). Right panels show pixel-by-pixel scatterplots of radiance for all coincident pixels, with line showing 1:1 relation.

(Fig. 17) suggests that the time difference is not the major source of this discrepancy.

The 'nominal'-spectral resolution VIRTIS measurements show consistent excess in received signal at wavelengths around 1.15 μm and 1.4 μm, whilst 'high spectral resolution' measurements imply that the differences at 1.15 μm are probably a result of spectral averaging over spectral bins — but confirm the discrepancies at 1.4 μm, ranging between 1.35 and 1.5 μm when the VIRTIS measurements are compared with coincident Earth-observing data, and radiative-transfer simulations.

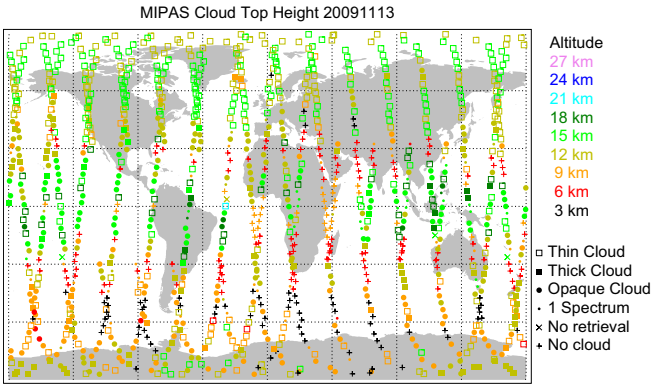

Fig. 21. Height of aerosol/cloud in the ENVISAT/MIPAS limb-scan pattern (credit: Anu Dudhia, University of Oxford), using the MIPclouds operational processor. Colours represent the height of the highest aerosol layer, and symbols indicate the opacity of cloud/aerosol.

It was considered whether the source of extraneous radiance was in fact a lack of sensitivity in the VIRTIS detectors. However, this was ruled out since VIRTIS measurements of Lutetia and Mars at 1.4 μm show radiances as small as 2 $\mu W\,cm^{-2}\,sr^{-1}\,\mu m^{-1}$.

At the time of the observation, the northern mid-latitude stratosphere was loaded with volcanic aerosol following the Sarychev Peak eruption in June 2009. Whilst the volcanic aerosol loading could explain the differences between NEMESIS simulations having 'normal' atmospheric trace species concentrations and aerosol loading, it cannot explain the differences between VIRTIS, and SCIAMACHY and MODIS. Although tropospheric clouds move slightly between the three datasets, which is to be expected since these are small and have sharp edges, volcanic aerosols at higher altitudes are much more smoothly distributed and it is inconceivable that VIRTIS should have seen a different aerosol field to both MODIS and SCIAMACHY, whose measurements are consistent with each other. Furthermore, as discussed in Section 6, at the time of these observations, the stratospheric aerosol opacity was much further north than the cloud-free ocean pixels considered, and thus it is extremely unlikely that there is, in fact, any volcanic aerosols measured by either of the compared instruments. Thus, the volcanic aerosols in the atmosphere cannot be

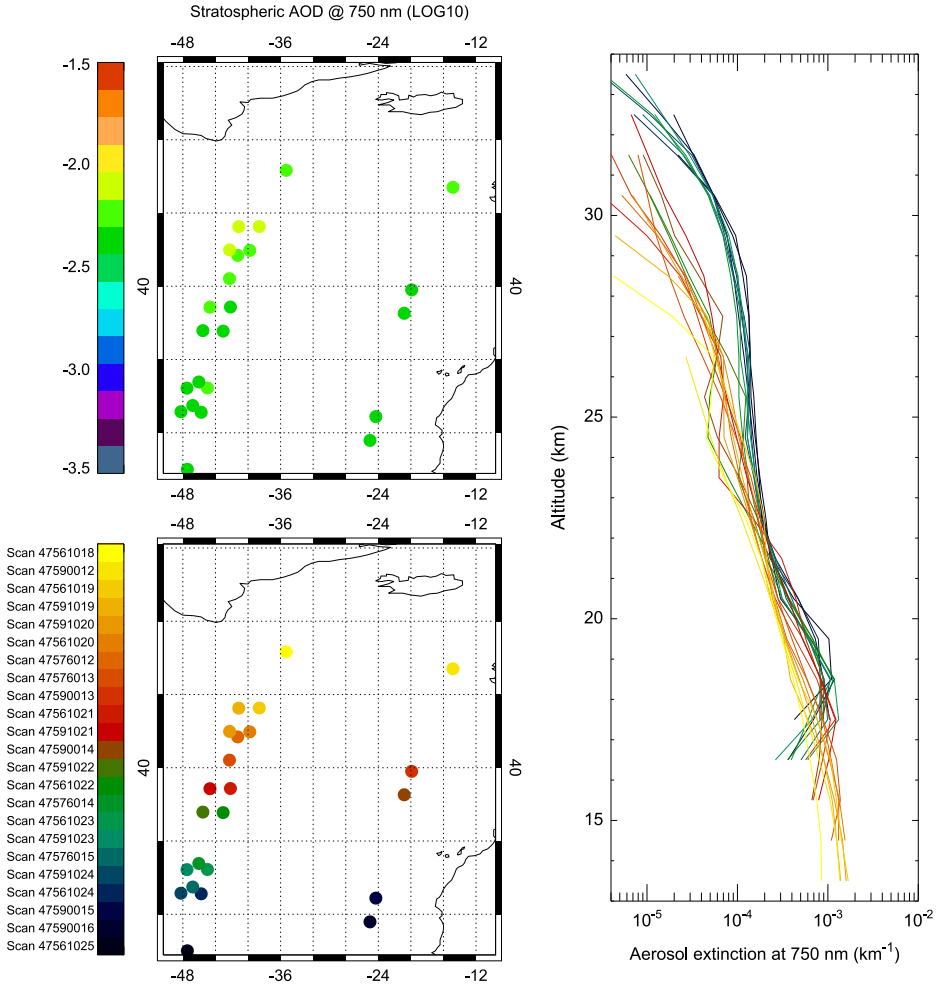

Fig. 22. OSIRIS stratospheric aerosol extinction for 13 November 2009. Top left panel: Optical depth at 750 nm in the stratosphere. Bottom left panel: Scan ID number geographic location. Right panel: Vertical aerosol extinction coefficient profile, colour-coded by scan ID number, at 750 nm.

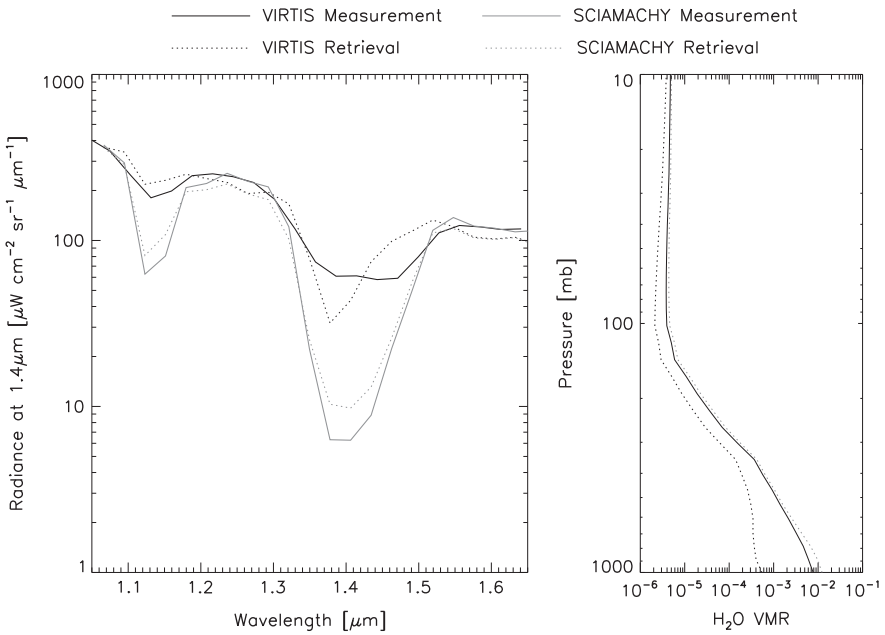

Fig. 23. Simulated (dotted lines) radiance spectra (left panel) when NEMESIS is used to retrieve the water vapour profile (right panel) from 'nominal mode' VIRTIS (black lines) and SCIAMACHY (grey lines) measurements (given in solid lines), for the same thin haze distribution.

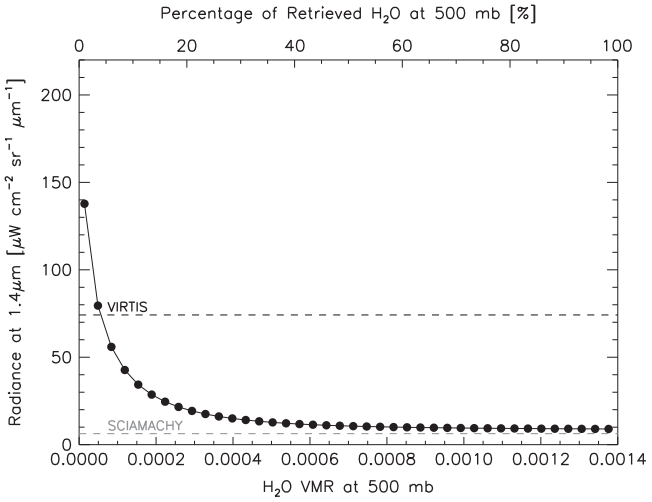

Fig. 24. NEMESIS simulated radiances at 1.4 μm for ocean input data, perturbing the tropospheric concentration of the water vapour as retrieved by SCIAMACHY for the case grid-box (solid lines, with points). Black dashed line shows the 'nominal mode' VIRTIS measurement from the grid-box, and grey dashed line shows SCIAMACHY measurement from the same grid-box.

the reason why VIRTIS radiances do not match SCIAMACHY and MODIS measurements.

Additionally, SCIAMACHY is known to suffer ice contamination — however, this is asserted to occur seriously in channels 7 and 8, whereas channels 1–6 are relatively unaffected. In this work, the VIRTIS radiances have been compared with SCIAMACHY's channel 6 radiances only, and ice contamination should not be an overriding issue in the resulting comparisons. This is furthermore confirmed by generally good correspondence between SCIAMACHY and MODIS radiances in the 1.4 μm region, except at a scattering of very low radiance cases, suggesting that SCIAMACHY is only slightly contaminated in channel 6. Thus, large-scale ice contamination on SCIAMACHY is asserted to not be the cause of the VIRTIS/SCIAMACHY discrepancy, except possibly at the lowest radiance cases.

The VIRTIS order-sorting filters are made in five joined sections covering the spectral ranges, and it is proposed that the first junction at 1.51 μm, affecting the signal from 1.415 μm to 1.594 μm, acts as reflector and re-distributes photons belonging to different wavelengths on pixels in the proximity of the filter junction (Filacchione et al., 2006). The artefacts introduced by the presence of the filter junction are normally removed by the calibration process; however, whenever strong radiance gradients are present in the image or in case of strong continuum signals on the band shoulders, the present spectral calibration is unable to remove them completely. A calibration residual can be seen in the high spectral resolution measurements where there is almost uniformly a 'bump' in the spectra at approximately 1.41 μm (Fig. 16). Although not previously observed in other VIRTIS measurements, it is possible that the 1.415–1.594 μm filter generates stray light outside its nominal range, resulting in bands outside those within the filter's geometrical range being affected by the light leak.

8. Comet spectra

Though there are wavelengths for which cometary spectra are dominated by continuum features, and are fairly spectrally flat rather than having distinct sharp absorption and emission features, in the VIRTIS wavelength region, there are very distinct water vapour, carbon dioxide and organic emissions, and water ice absorptions (e.g. Feaga et al., 2007), as observed by Deep Impact HRI-IR. In fact, Deep Impact's HRI-IR indicates that there is very little continuum in the 1.4–4.5 μm region of comets which does not include gaseous absorption/emission. The Deep Impact mission is currently analysing cometary spectra in the 1–4.8 μm range, and should shed light upon the excited-state population and absorption/emission spectrum of water vapour in a non-collisional free-space environment (e.g. A'Hearn et al., 2011). The Deep Impact findings corroborated the observations taken of comet Halley (Combes et al., 1988) which certainly showed distinct gaseous emission lines. Furthermore, the AKARI spacecraft sampled many comets in the infrared, and reports distinct H_2O,

CO_2 and CO emission features in the 2.5–5 μm spectral region (e.g. Ootsubo et al., 2012).

The spectral characteristics of comets are likely to evolve and change along the cometary orbit, as the comet moves from cold, deep space towards the Sun, and the emission of volatiles begins, with the formation of the coma — and VIRTIS' scientific objectives focus on the study of the formation and evolution of the coma and of its gaseous and dusty components (Coradini et al., 1998). It thus seems likely that the spectra of comet 67P/Churyumov–Gerasimenko should exhibit sharp absorptions/emissions in the Rosetta/VIRTIS wavelength range.

Thus, with the current documented and published knowledge on cometary spectroscopy, it is impossible to tell the impact which light leakages in the water absorption regions within 1–5 μm will have on measured cometary spectra, regardless of the source of the errors — although it is clear that the comet 67P/Churyumov–Gerasimenko spectra shall indeed exhibit sharp absorption/emission lines in the wavelength region in which Rosetta/VIRTIS is suspected to have light leaks. It is also reasonable to expect that some of the comet observations — especially those at 3 AU — will have very low radiances, so it is important that the discrepancies in the VIRTIS data at 1.15 μm and 1.4 μm are corrected or better calibrated. Although this is beyond the scope of this paper, this is necessary and important future work. A natural starting point would be to use the Earth observation comparison data to validate such a scaling or correction in order to account for the scattered light.

However, VIRTIS behaves well and reliably throughout most of its measured spectral range, and over the vast majority of observation conditions, and will regardless deliver high-impact and high-value new comet science.

9. Conclusions

In this work, Rosetta/VIRTIS observations of Earth taken in November 2009 have been compared with near-coincident data taken by Earth-observing instruments (ENVISAT/AATSR, TERRA/MODIS and ENVISAT/SCIAMACHY), as well as with radiative-transfer simulations by multi-scattering tool NEMESIS. An important lesson learnt is to avoid acquisition in the 'nominal' spectral mode in order to achieve the best possible science, which has now been implemented in the operation plan in favour of high spatial/spectral mode observations. Overall, on a statistically significant level, Rosetta/VIRTIS measurements have a 90% correlation with AATSR observations, between 85% and 94% correlation with MODIS observations, and between 82% and 88% correlation with SCIAMACHY observations. There are consistent differences between VIRTIS and the Earth-observing instruments MODIS and SCIAMACHY at the deep water vapour absorption feature at 1.4 μm over cloud-free pixels (regions where the expected magnitudes of the signal are fairly low, in comparison with cloudy measurements), in which VIRTIS appears to measure more radiance than do both SCIAMACHY and MODIS, which are mostly consistent, with SCIAMACHY occasionally registering lower radiances than MODIS. The presence of an order sorting filter on the VIRTIS detector located over the spectral region 1.415–1.594 μm could imply spurious reflections and light leaks within the 1.4 μm water band for low radiance levels. VIRTIS' behaviour in the spectral region of 1.4 μm warrants further study to confirm this possible discrepancy in view of the upcoming exciting year long mission at the comet 67P/Churyumov–Gerasimenko where VIRTIS shall measure visible and infrared spectra of the cometary nucleus surface as well as coma gas and dust.

Acknowledgements

The authors would like to thank Lori M. Feaga (University of Maryland) and Timothy A. Livengood (NASA/Goddard Space Flight Center) for helpful conversations about comet spectra, and Anu Dudhia and Don Grainger (AOPP/Oxford) for helpful discussions on stratospheric aerosols. SCIAMACHY data was provided by the European Space Agency under the Category-1 Proposal C1P.8489. Rosetta/VIRTIS is a project funded by the Italian Space Agency.

References

A'Hearn, M.F., Belton, M.J.S., Delamere, W.A., Feaga, L.M., Hampton, D., Kissel, J., Klaasen, K.P., McFadden, L.A., Meech, K.J., Melosh, H.J., Schultz, P.H., Sunshine, J. M., Thomas, P.C., Veverka, J., Wellnitz, D.D., Yeomans, D.K., Besse, S., Bodewits, D., Bowling, T.J., Carcich, B.T., Collins, S.M., Farnham, T.L., Groussin, O., Hermalyn, B., Kelley, M.S., Li, J.-Y., Lindler, D.J., Lisse, C.M., McLaughlin, S.A., Merlin, F., Protopapa, J.L., Richardson, J.E., Williams, J.L., 2011. Science 332 (6036), 1396–-1400, http://dx.doi.org/10.1126/science.1204054.

Ammannito, E., Filacchione, G., Coradini, A., Capaccioni, F., Piccioni, G., Sanctis, M.C. D., 2006. On-ground characterization of Rosetta/VIRTIS-M. i. spectral and geometrical calibrations. Rev. Sci. Instrum. 77, 093109.

Baldridge, A.M., Hook, S.J., Grove, C.I., Rivera, G. The ASTER Spectral Library Version 2.0. Rem. Sens. Environ. 9, in press.

Bourassa, A., Robock, A., Randel, W., Deshler, T., Rieger, L., Lloyd, N., Llewellyn, E., Degenstein, D., 2012. Large volcanic aerosol load in the stratosphere linked to asian monsoon transport. Science 337 (6090), 78–81.

Burrows, J., Hölzle, E., Goede, A.P.H., Visser, H., Fricke, W., 1995. SCIAMACHY—scanning imaging absorption spectrometer for atmospheric chartography. Astron. Astrophys. 35, 445–451.

Combes, M., Moroz, V., Crovisier, J., Encrenaz, T., Bibring, J.P., Grigoriev, A.V., Sanko, N.F., Coron, N., Crifo, J.F., Gispert, R., Bockelee-Morvan, D., Nikolsky, V.Y., Krasnopolsky, V.A., Owen, T., Emerich, C., Lamarre, J.M., Rocard, F., 1988. The 2.5 to 12 μm spectrum of comet Halley from the IKS-VEGA experiment. Icarus 76, 404–436.

Coradini, A., Capaccioni, F., Drossart, P., Semery, A., Arnold, G., Schade, U., Angrilli, F., Barucci, M.A., Bellucci, G., Bianchini, G., Bibring, J.P., Blanco, A., Blecka, M., Bockelee-Morvan, D., Bonsignori, R., Bouye, M., Bussoletti, E., Capria, M.T., Carlson, R., Carsenty, U., Cerroni, P., Colangeli, L., Combes, M., Combi, M., Crovisier, J., Dami, M., DeSanctis, M.C., DiLellis, A.M., Dotto, E., Encrenaz, T., Epifani, E., Erard, S., Espinasse, S., Fave, A., Federico, C., Fink, U., Fonti, S., Formisano, V., Hello, Y., Hirsch, H., Huntzinger, G., Knoll, R., Kouach, D., Ip, W.H., Irwin, P., Kachlicki, J., Langevin, Y., Magni, G., McCord, T., Mennella, V., Michaelis, H., Mondello, G., Mottola, S., Neukum, G., Orofino, V., Orosei, R., Palumbo, P., Peter, G., Pforte, B., Piccioni, G., Reess, G.M., Ress, E., Saggin, B., Schmitt, B., Stefanovitch, Stern, A., Taylor, F., Tiphene, D., Tozzi, G., 1998. Virtis: an imaging spectrometer for the rosetta mission. Planet. Space Sci. 46 (9–10), 1291–1304.

Coradini, A., Capaccioni, F., Drossart, P., Arnold, G., Ammannito, E., Angrilli, F., Barucci, A., Bellucci, G., Benkhoff, J., Bianchini, G., Bibring, J.P., Blecka, M., Bockelee-Morvan, D., Capria, M.T., Carlson, R., Carsenty, U., Cerroni, P., Colangeli, L., Combes, M., Combi, M., Crovisier, J., Desanctis, M.C., Encrenaz, E.T., Erard, S., Federico, C., Filacchione, G., Fink, U., Fonti, S., Formisano, V., Ip, W.H., Jaumann, R., Kuehrt, E., Langevin, Y., Magni, G., Mccord, T., Mennella, V., Mottola, S., Neukum, G., Palumbo, P., Piccioni, G., Rauer, H., Saggin, B., Schmitt, B., Tiphene, D., Tozzi, G., 2007. Virtis: an imaging spectrometer for the Rosetta mission. Space Sci. Rev. 128, 529–559.

Coradini, A., Grassi, D., Capaccioni, F., Filacchione, G., Tosi, F., Ammannito, E., De Sanctis, M.C., Formisano, V., Wolkenberg, P., Rinaldi, G., Arnold, G., Barucci, M. A., Bellucci, G., Benkhoff, J., Bibring, J.P., Blanco, A., Bockelee-Morvan, D., Capria, M.T., Carlson, R., Carsenty, U., Cerroni, P., Colangeli, L., Combes, M., Combi, M., Crovisier, J., Drossart, P., Encrenaz, T., Erard, S., Federico, C., Fink, U., Fonti, S., Ip, W.-H., Irwin, P.G.J., Jaumann, R., Kuehrt, E., Langevin, Y., Magni, G., McCord, T., Mennella, V., Mottola, S., Neukum, G., Orofino, V., Palumbo, P., Piccioni, G., Rauer, H., Schmitt, B., Tiphene, D., Taylor, F.W., Tozzi, G.P., 2010. Martian atmosphere as observed by VIRTIS-M on Rosetta spacecraft. J. Geophys. Res. 115, E04004.

Coradini, A., Capaccioni, F., Erard, S., Arnold, G., De Sanctis, M.C., Filacchione, G., Tosi, F., Barucci, M.A., Capria, M.T., Ammannito, E., Grassi, D., Piccioni, G., Giuppi, S., Bellucci, G., Benkhoff, J., Bibring, J.P., Blanco, A., Blecka, M., Bockelee-Morvan, D., Carraro, F., Carlson, R., Carsenty, U., Cerroni, P., Colangeli, L., Combes, M., Combi, M., Crovisier, J., Drossart, P., Encrenaz, E.T., Federico, C., Fink, U., Fonti, S., Giacomini, L., Ip, W.-H., Jaumann, R., Kuehrt, E., Langevin, Y., Magni, G., McCord, T., Mennella, V., Mottola, S., Neukum, G., Orofino, V., Palumbo, P., Schade, U., Schmitt, B., Taylor, F., Tiphene, D., Tozzi, G., 2011. The surface composition and temperature of asteroid 21 lutetia as observed by Rosetta/VIRTIS. Science 334, 492–494.

ESA, 2008. Level 1b Product Quality Disclaimer, ENVI-GSOP-EOGD-QD-10-0097.

Feaga, L.M., A'Hearn, M.F., Sunshine, J.M., Groussin, O., Farnham, T.L., 2007. Asymmetries in the distribution of {H_2O} and {CO_2} in the inner coma of Comet 9P/Tempel 1 as observed by Deep Impact. Icarus 190 (2), 345–356.

Filacchione, G., Ammannito, E., Coradini, A., Capaccioni, F., Piccioni, G., Sanctis, M.C. D., Dami, M., Barbis, A., 2006. On-ground characterization of rosetta/virtis-m. ii. spatial and radiometric calibrations. Rev. Sci. Instrum. 77, 103106.

Giuppi, S., Coradini, A., Capaccioni, F., Capria, M.T., De Sanctis, M.C., Erard, S., Filacchione, G., Tosi, F., Ammannito, E., 2011. Performances of the data compression and binning algorithms adopted on the VIRTIS-M spectrometer onboard rosetta. In: EPSC-DPS Joint Meeting 2011, 2–7 October 2011 in Nantes, France. 2011epsc.conf.514G.

Goody, R., West, R., Chen, L., Crisp, D., 1989. The correlated-k method for radiation calculations in nonhomogeneous atmospheres. J. Quant. Spectrosc. Radiat. 42, 539–550.

Hurley, J., Dudhia, A., Grainger, R.G., 2011. Retrieval of macrophysical cloud parameters from MIPAS: algorithm description. Atmos. Meas. Tech. 4, 683–704.

Irwin, P., Teanby, N., de Kok, R., Fletcher, L., Howett, C., Tsang, C., Wilson, C., Calcutt, S., Nixon, C., Parrish, P., 2008. The NEMESIS planetary atmosphere radiative transfer and retrieval tool. J. Quant. Spectrosc. Radiat. Transf. 109 (6), 1136–1150.

King, M.D., Kaufman, Y.J., Menzel, W.P., Tanré, D., 1992. Remote sensing of cloud, aerosol, and water vapor properties from the Moderate Resolution Imaging Spectrometer (MODIS). IEEE Trans. Geosci. 30, 2–27.

Lacis, A., Oinas, V., 1991. A description of the correlated-k distribution method for modelling nongray gaseous absorption, thermal emission, and multiple scattering in vertically inhomogeneous atmospheres. J. Geophys. Res. 96 (15), 9027–9064.

Langevin, Y., Forni, O., 2000. Image and spectral image compression for four experiments on the ROSETTA and Mars Express missions of ESA. Proc. SPIE 4115, 364–373. (in Applications of Digital Image Processing XXIII, Andrew G. Tescher (editor)).

Llewellyn-Jones, D., Edwards, M., Mutlow, C., Birks, A., Barton, I., Tait, H., 2001. AATSR: global-change and surface-temperature measurements from envisat. ESA Bull. 105, 10–21.

Marceau, D., Howarth, P., Gratton, D., 1994. Remote sensing and the measurement of geographical entities in a forest environment. 1: the scale and spatial aggregation problem. Remote Sens. Environ. 49, 93–104.

Nelson, M., McRoberts, R., Holden, G., Bauer, M., 2009. Effects of satellite image spatial aggregation and resolution on estimates of forest land area. Int. J. Remote Sens. 30, 1913–1940.

Ootsubo, T., Kawakita, H., Hamada, S., Kobayashi, H., Yamaguchi, M., Usui, F., Nakagawa, T., Ueno, M., Ishiguro, M., Sekiguchi, T., Watanabe, J., Sakon, I., Shimonishi, T., Onaka, T., 2012. AKARI near-infrared spectroscopic survey for CO_2 in 18 comets. J. Astrophys. 752, 15, http://dx.doi.org/10.1088/0004-637X/752/1/15.

Rakwatin, P., Takeuchi, W., Yasuoka, Y., 2007. Stripe noise reduction in MODIS data by combining histogram matching with facet filter. IEEE Trans. Geosci. Remote Sens. 45 (6), 1844–1856.

Remedios, J., 2001. Profiles for MIPAS. EOS, Space Research Centre, Leicester, UK.

Rothman, L., Jacquemart, D., Barbe, A., Benner, D.C., Birk, M., Brown, L., Carleer, M., Jr., Chackerian, C., Chance, K., Coudert, L., Dana, V., Devi, V., Flaud, J.-M., Gamache, R., Goldman, A., Hartmann, J.-M., Jucks, K., Maki, A., Mandin, J.-Y., Massie, S., Orphal, J., Perrin, A., Rinsland, C., Smith, M., Tennyson, J., Tolchenov, R., Toth, R., Auwera, J.V., Varanasi, P., Wagner, G., 2005. The HITRAN 2004 molecular spectroscopic database. J. Quant. Spectrosc. Radiat. Transf. 96 (2), 139–204.

Sayer, A.M., Thomas, G.E., Grainger, R.G., 2010. A sea surface reflectance model for (A)ATSR, and application to aerosol retrievals. Atmos. Meas. Tech. 3, 813–838.

Tosi, F., Coradini, A., Capaccioni, F., Filacchione, G., Grassi, D., de Sanctis, M.C., Capria, M.T., Barucci, M.A., Fulchignoni, M., Mottola, S., Erard, S., Dotto, E., Baldetti, C., 2010. the VIRTIS Team, 2010. The light curve of asteroid 2867 Steins measured by VIRTIS-M during the Rosetta fly-by. Planet. Space Sci. 58, 1066–1076, http://dx.doi.org/10.1016/j.pss.2010.03.019.

Tosi, F., Capaccioni, F., Coradini, A., Erard, S., Filacchione, G., de Sanctis, M.C., Capria, M.T., Giuppi, S., Carraro, F., 2012. the VIRTIS Team, 2012. The light curve of asteroid 21 Lutetia measured by VIRTIS-M during the Rosetta fly-by. Planet. Space Sci. 66, 9–22, http://dx.doi.org/10.1016/j.pss.2011.11.016.